On the feasibility of axial injection in
superconducting cyclotrons

G. Bellomo, D. Johnson, F. Marti and F.G. Resmini

National Superconducting Cyclotron Laboratory

Michigan State University, East Lansing, MI   48824

Abstract

In connection with the superconducting cyclotron program
at M.S.U. a feasibility study of axial injection, aimed
mainly at the K-800 cyclotron, has been carried out.

The results encompass all major aspects of a working
system, i.e. center region, injection trajectories and phase
space matching. It is shown that axial injection is indeed
feasible, although problems exist not ordinarily encountered
in conventional A.V.F. cyclotrons.

The possible solutions and limitations are presented
and discussed in detail.

Introduction

A large amount of research and development has been carried out recently in various laboratories, concerning new types of heavy ion sources for accelerators. Noteworthy results have already been reported for EBIS[1] and E.C.R.[2] sources. Both of these sources, although using quite different physical principles, aim at producing high charge states for light-medium, and more in perspective, very heavy ions.

Even though a substantial development work must still be carried out, the results so far obtained are very encouraging. In particular, it looks like the E.C.R. source is already at the stage where high charge states of ions up to mass ≈ 40 can be produced with reasonable intensities. This fact has enticed several laboratories with A.V.F. cyclotrons[3,4,5,6,7] to provide themselves with such sources which will be used via an axial injection system.

In connection with the superconducting cyclotron program at M.S.U., we have undertaken a feasibility study of axial injection into superconducting cyclotrons. Axial injection at moderate injection voltages (tens of kV at most) seems in fact the most practical way to use these sources also in superconducting cyclotrons. The advantages of such source with respect to the conventional PIG sources seem, on paper, impressive enough in terms of either intensities or high charge states to warrant such a study.

The goal of the present investigation was not to produce a detailed design of an actual axial injection system, but

rather to identify the main physical problems and find out realistic solutions. The peculiar characteristics of superconducting cyclotrons, like the very high magnetic fields, limited clearances in the center etc., suggest in fact that problems may be more complex than those already solved in conventional A.V.F. cyclotrons.

In the process we have obtained results which do have a general validity and should therefore hold for any superconducting cyclotron where axial injection is attempted. It is the purpose of this paper to present them in some detail.

1. General Outline

This study has been mostly connected with the K-800 cyclotron, whose design parameters are extensively reported elsewhere.[8] For the sake of clarity, Fig. 1 shows the operating diagram of the cyclotron in the $(B_0, q/A)$ plane, B_0 being the center field value and q/A the charge to mass ratio of the ion accelerated. In this context we have chosen the following two representative ions:

-   a fully stripped light ion, $q/A=.5$, with a center field B_0 of 34.6 kgauss, which corresponds to an energy of 200 MeV/n.
-   a high charge state (46^+) uranium ions, at a center field B_0 of 47.5 kgauss, with a final energy of 45 MeV/n.
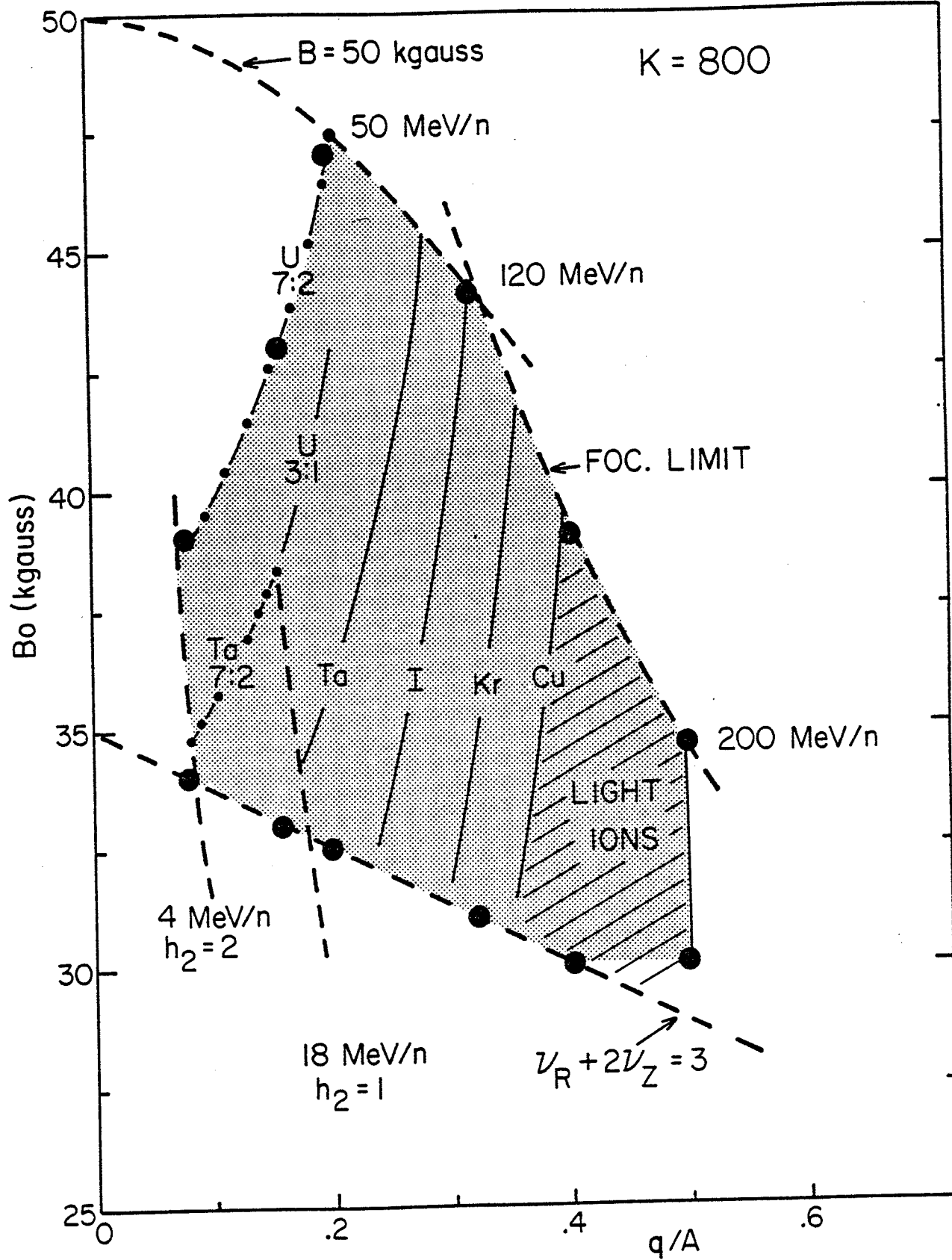
FIG. 1. Operating diagram of the K-800 cyclotron in the (B_o, q/A) plane.

As will be apparent later, the analysis of these two cases encompasses, at least from the point of view of magnetic field properties, most of the machine operating range.

The axial injection scheme is presented in Fig. 2 just to show the physical dimensions involved. Since a detailed analysis of the single components and their purposes is made later on, only a few comments are in order:

i) The injection is assumed to start at z = 100" from the median plane, where the magnetic field produced by the cyclotron is practically zero. Farther away, therefore, "conventional" beam optics is assumed.

ii) Proper matching to the cyclotron acceptance, and adequate beam transmission through the axial hole can be achieved either with a long solenoid, or a couple of einzel lenses (see Sect. 4, 5). A set of deflectors (see Sec. 3) is needed to steer the beam off axis before it enters the plug.

iii) For the purpose of the present study, an electrostatic mirror[9,10] has been selected as inflector of the injected beams into the median plane. Although other types of inflectors, like hyperboloid-shaped channels[11,12] have been proposed and actually used in A.V.F. cyclotrons, the mirror seemed to us, for the time being, quite advantageous both because of its straightforward operating mode and easy construction.

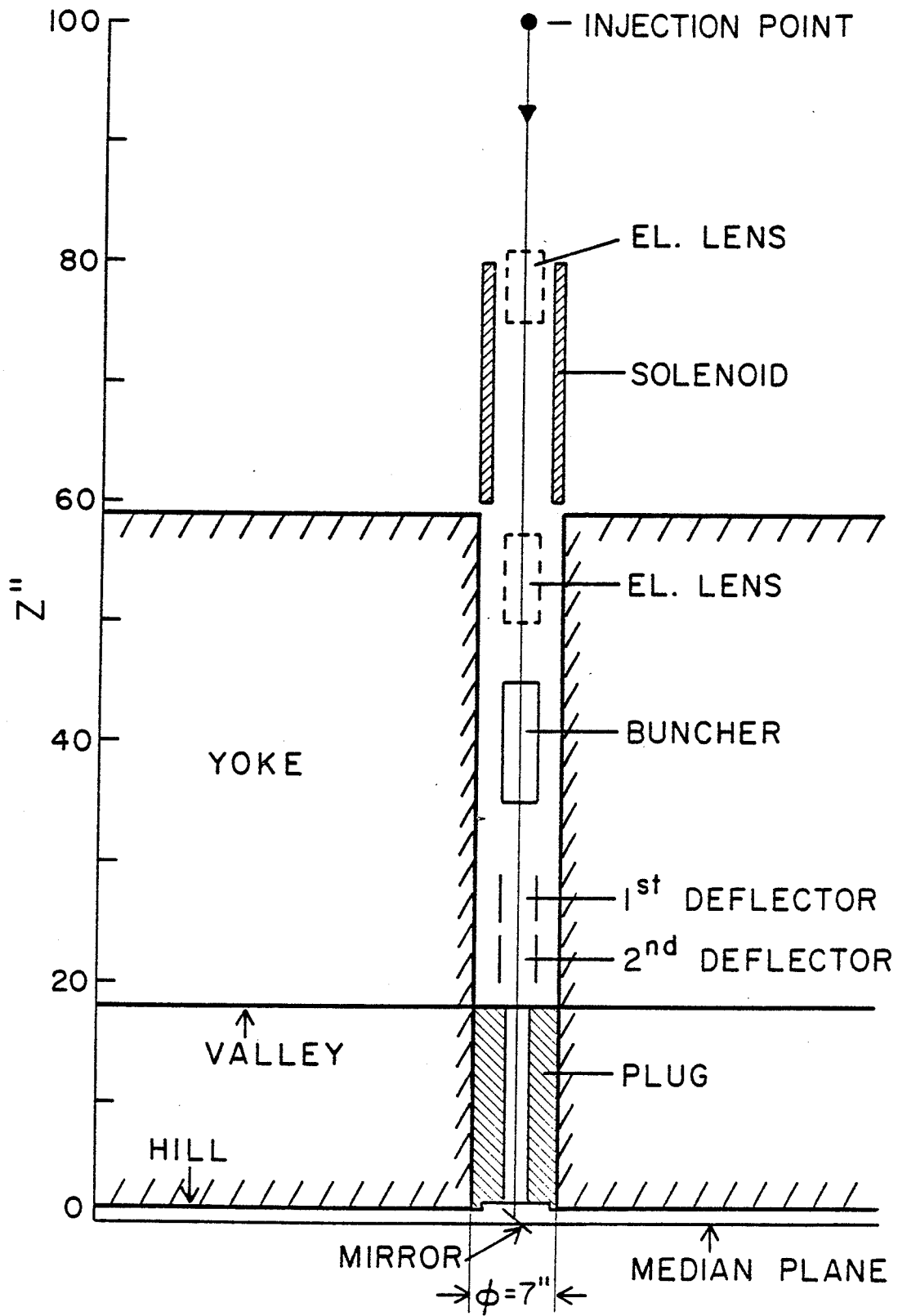Scaling of the trajectories throught the mirror demands that (See App. A):

FIG. 2. Conceptual axial injection scheme.

$$\rho = \frac{p}{qB_o} = \left(\frac{2\ V_{inj}}{\frac{q}{Am_o}\ B_o^2}\right)^{\frac{1}{2}} = \text{const} \qquad (1)$$

where ρ is the curvature radius, V_{inj} the injection voltage, B_o and q/A have been just defined. The values of ρ, at different injection voltage, for the two representative ions chosen, are listed in Table I.

Consequently the beam transmission, and phase space matching have been investigated at V_{inj} = 15, 20, 25 kV for the q/A=.5 ion and correspondingly at 10, 15, 20 kV for the 46^+ uranium ion. The choice of an upper limit around 25-30 kV avoids too high voltages on the mirror, given the available clearances. The factor of two voltage variation ensures that beam optics does not depend critically upon the injection energy, which can therefore be chosen subsequently on the basis of other criteria.

We now discuss first the selection of a suitable center region geometry, and turn thereafter to the problems associated with the injection itself.

2. The central region

A full analytical treatment of the mirror, including the effects of inflection on the phase space is given in App. A. Mirror parameters have been chosen by taking as reference case the q/A=.5 ion, injected at 20 kV in the field B_o = 34.6 kgauss with a corresponding ρ = 8.322 mm. By posing an upper limit of 50 kV/cm for the electric field in the mirror, the following parameters are obtained:

- angle of the mirror grid with the median plane $\alpha = 47.5^{\circ}$
- distance between grid and electrode D = 3.75 mm
- mirror voltage V = 18.6 kV
- Distance from the injection axis to the exit point, projected on the median plane, R_D = 6.15 mm.

With these discussions, the mirror structure consists of an outer cylindrical shell, at ground potential, of 25 mm outer diameter, and 1.5 mm thick walls. A 3 mm clearance exists between this shell and the high voltage electrode, which has thus a 16 mm diameter.

These dimensions have been used in connection with the center region studies. We recall that the accelerating structure of either the K = 500 or K = 800 machine consists of three dees in the valleys. Consequently, clearances to ground are very tight and the problem of designing a center region geometry which produces a centered beam usually requires a number of iterative steps. We refer to (13) for further details on the center region when an internal ion source is used. In the case of the axial injection the key issues, once the mirror is selected as inflector, are:

i) whether the latter can be positioned on the axis of the magnet, or off the axis, in order to get a centered beam.

ii) the range of injection voltages compatible with a centered beam, clearing all electrodes existing in the center.

In this context the present center region studies are of rather qualitative nature, just to provide answers to the questions above. Nevertheless, electrolytic tank measurements had to be carried out, in order to have a realistic mapping of the electric field.

Two main geometries were tried, i.e. either with the mirror on the magnet axis, or off the axis. It is assumed that a 100 kV peak dee voltage will be used, which requires at least 1 cm (or 1/2") clearance between electrodes.

We did not find any good solution with a mirror centered on the axis. An example of such a geometry is shown in Fig. 3, for a q/A=.5 particle, at an injection voltage of 20 kV. Although the center ray is centered within a few tenths of mm after several revolutions, this solution looks unrealistic, because the ion spends almost an entire revolution in the region between mirror and electrodes, being subject there to large transversal electric fields. This gives rise to instabilities as a function of the starting phase.

One cannot rule out, of course, that with a totally different geometry or else raising considerably the injection energy, a more realistic solution can be obtained. We did prefer, however, to investigate the possibility of off-axis injection also because the latter presents problems not usually encountered in conventional A.V.F. cyclotrons.

Off-axis injection proved in fact successful. Examples with a 25 mm diameter mirror, off-axis by about 10 mm, are shown in Figs. 4, 5, 6, for the q/A=.5 ion, at three different injection voltages of 10, 20, 30 kV respectively. A centered
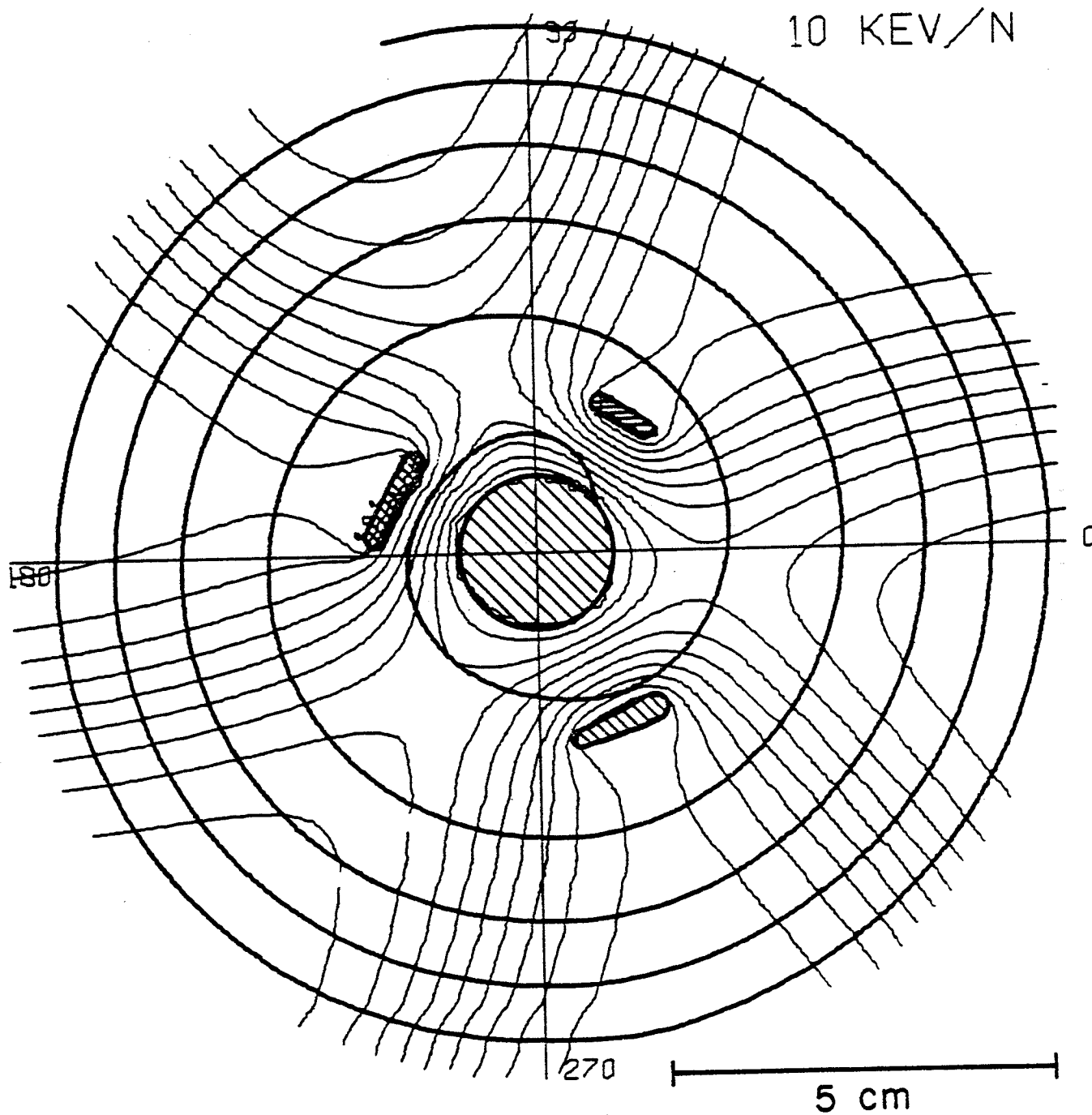
FIG. 3. On axis injection: center ray trajectory for
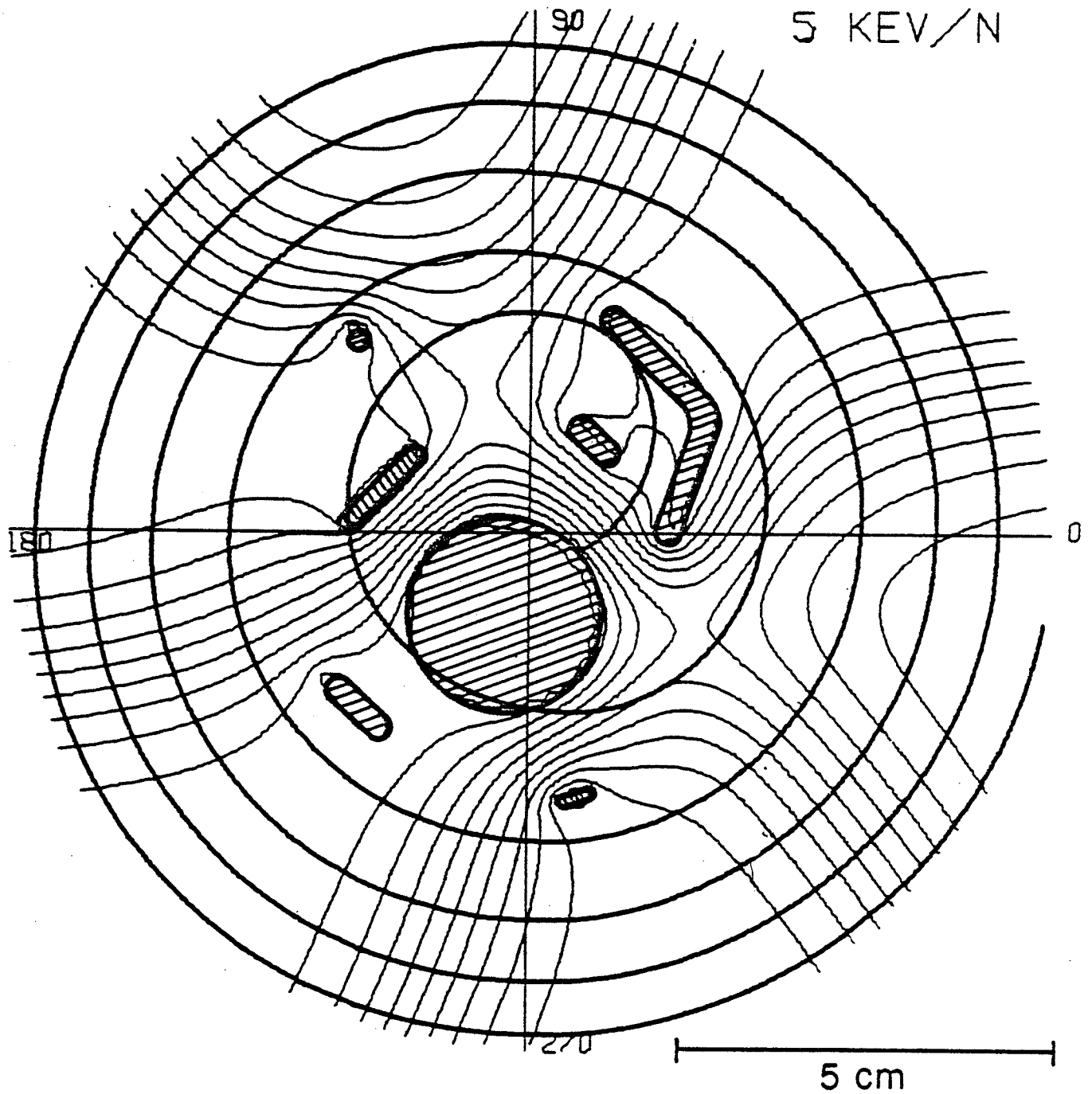a q/A = 0.5 ion, injected at 10 keV/n.

FIG. 4. Off-axis injection: center ray trajectory for
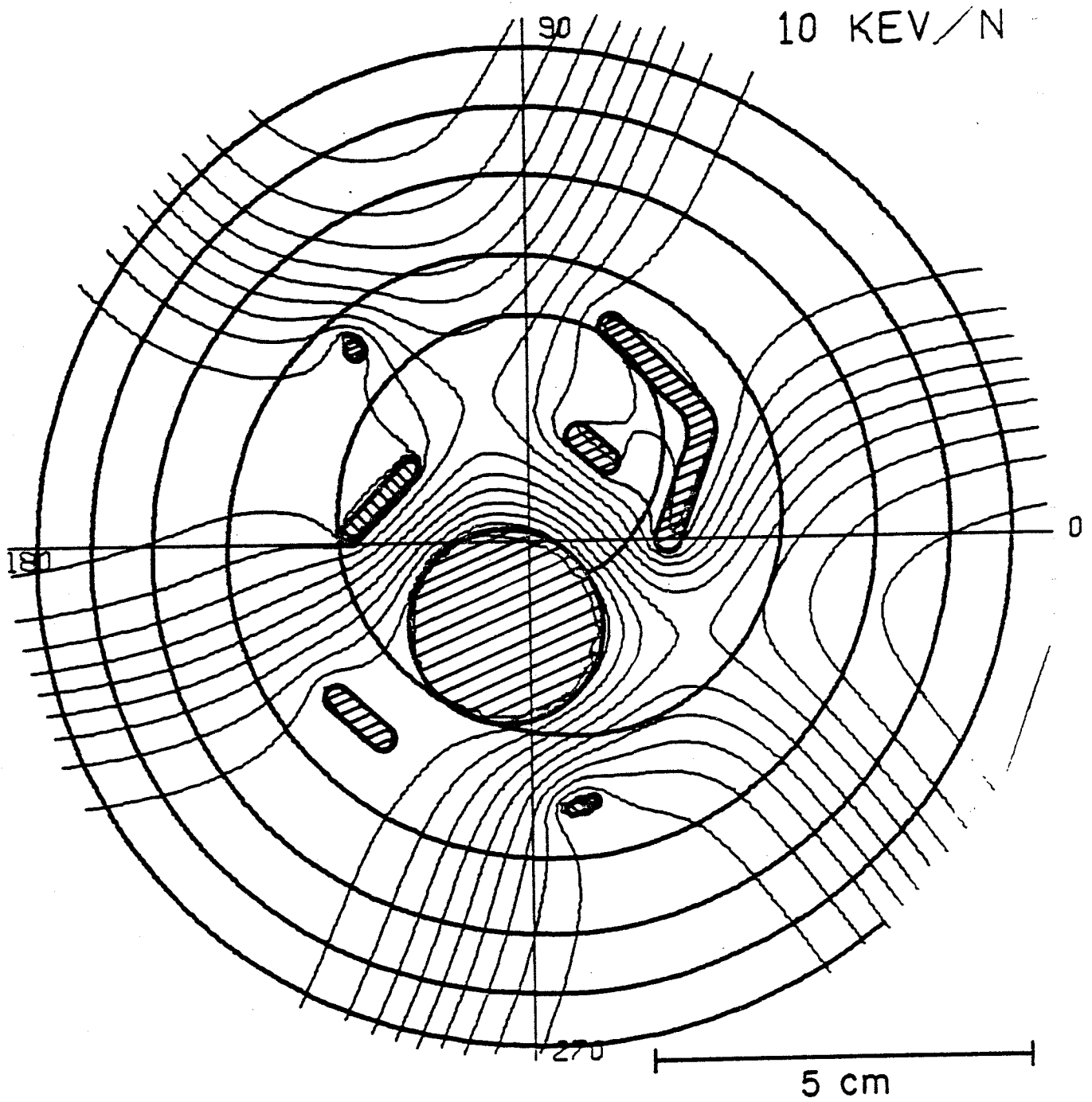a q/A = 0.5 ion, injected at 5 keV/n.

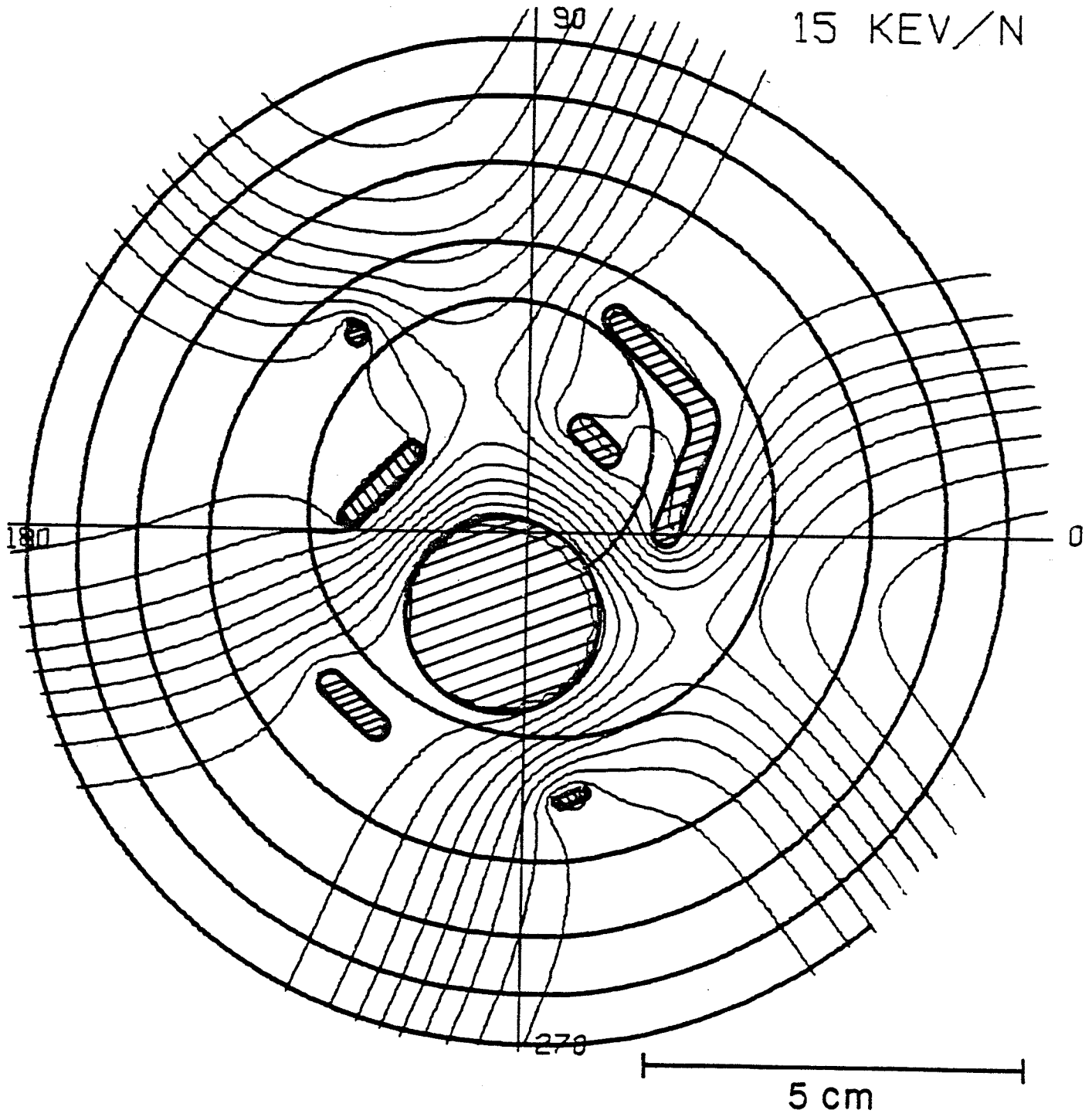FIG. 5.   Similar to Fig. 4, but injected at 10 keV/n.

FIG. 6. Similar to fig. 4, but injected at 15 keV/n.

beam is obtained in all cases, but it is clear that 20 kV,
for this particular ion, is close to the lower practical
limit for clearing the mirror.

It should be remarked that the center region presented
here has been adapted, for use with the off-axis mirror,
from the one used with the internal ion source. No optimi-
zation effort has been made and it could certainly be improved.

Therefore, even though these data on the central region
should be considered as only qualitative, it's clear that:

- off-axis injection looks more favorable if a mirror
  is used.
- the off the axis displacement is of the order of 10-
  12 mm at most.
- the range of useful injection voltages, for the $Q/A=.5$
  ion is probably between 15 and 30 kV. The voltages
  for all other ions can be obtained by scaling according
  to eq. 1.

3. Beam injection

3.1 The magnetic field in the hole

The conclusion, from center region studies, that off-
axis injection is perhaps necessary raises the question
of how this can be accomplished, if at all.

In fact the magnetic field along an axial hole in a
superconducting cyclotron is very different from that of
conventional A.V.F. cyclotrons. This can be seen in Fig. 7,

where the fields for several coil excitations, are plotted as a function of the distance z from the median plane. These fields are calculated with the program TRIM[14] and should be accurate to better than 1%. The geometry to which these calculations refer is shown in the figure itself. It corresponds to the one of Fig. 2, except for the center plug length, which extends only up to 11.5" from the median plane.

As seen from the curves of Fig. 7, the field is characterized by a sharp gradient near the median plane, as in conventional A.V.F. cyclotrons, and by another sharp peak at the plug end. Afterwards the field decreases almost linearly along the axis, until another peak, this one of small amplitude, is found at the yoke exit.

The analysis of the various contributions to this peculiar field behavior is presented for one excitation only in Fig. 8. The long linear "tail" comes from the coils themselves, while the plug is responsible for the sharp peaks up to 12" from the median plane. The rapid field decrease between 12"-14" and 20" is due instead to the yoke.

3.2 Center ray trajectories

The gradient of B_z along the axis gives rise to a B_r component, off the axis, which to first order can be written as
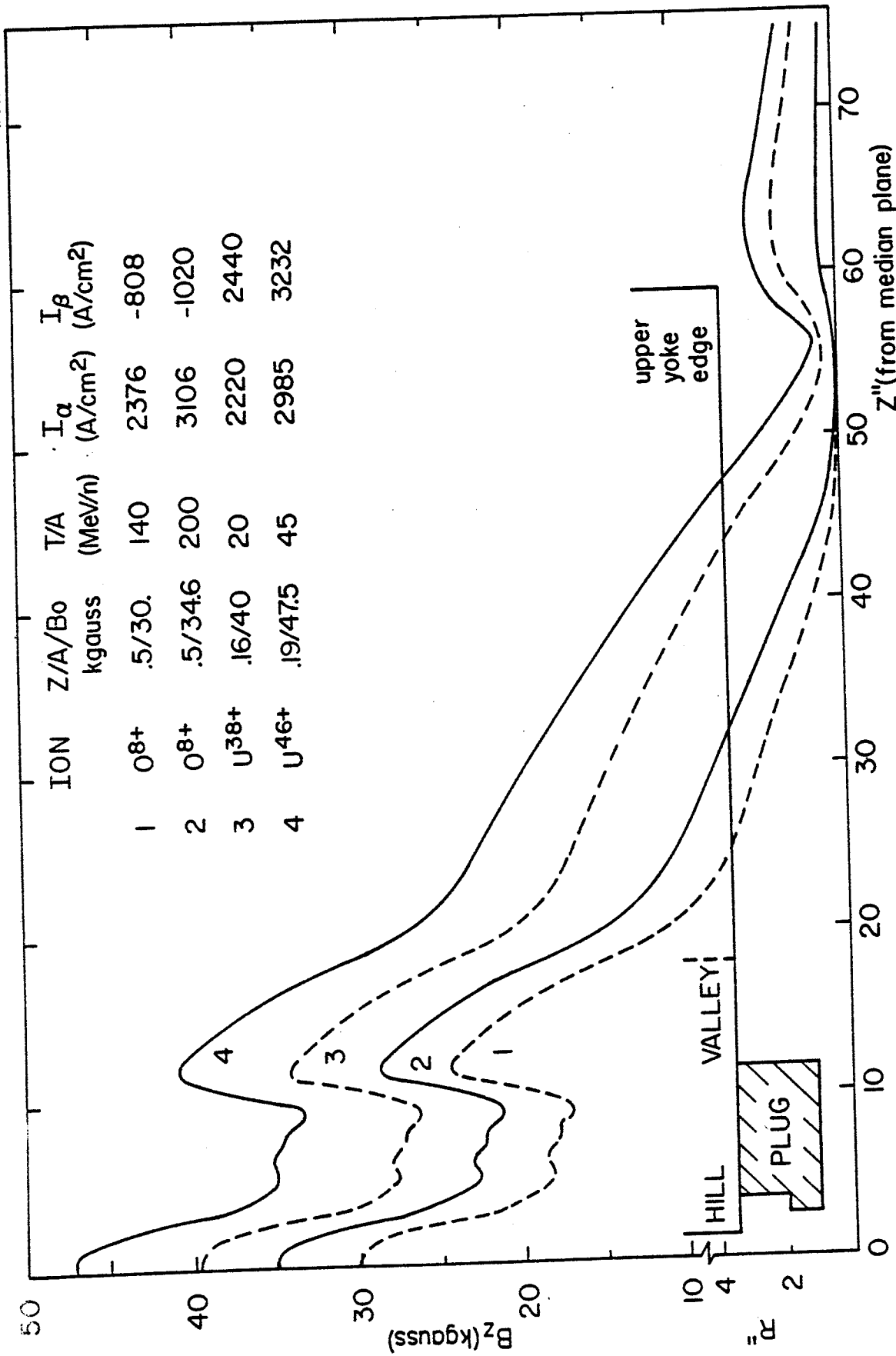
9

FIG. 7. Magnetic field along the cyclotron axial hole
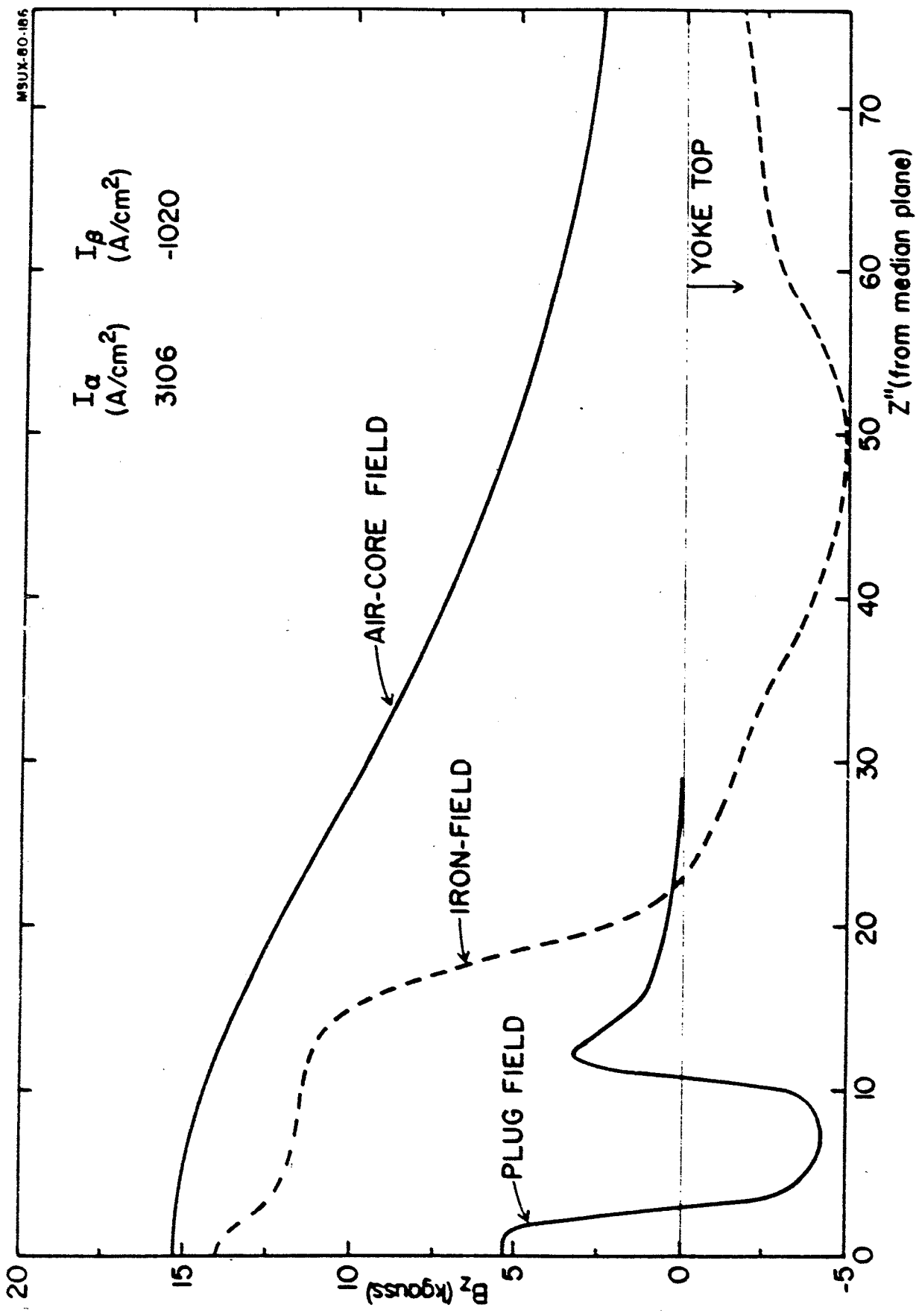for the excitations corresponding to the four ions listed.

FIG. 8. Partial contributions to the total field No. 2 of Fig. 7.

$$B_r = -\frac{r}{2}\frac{\partial B_z}{\partial z} \qquad (2)$$

were r is the radial distance from the axis.

The existence of strong B_r components all along the hole, as apparent from the curves of Fig. 7, establishes a magnetic axis essentially coincident with the coils axis and which cannot be displaced.

Attempts to inject the beam off-axis without correcting the center-ray trajectories are therefore bound to fail. Typically a center-ray with $p_z = p$ and 10 mm off the axis at z = 0", as required for proper injection, when traced backwards up to z = 100" is 20-25 mm further away off the axis, with both p_x and p_y different from zero, and (x,y) coordinates dependent upon the particle energy. Therefore a special scheme must be devised for injecting the beam off the axis at the median plane. The simplest one, and the one we have studied in detail, envisages a beam injection along the magnet axis, until close to the plug entrance. At that point a suitable set of deflectors, as sketched in Fig. 2, swings the beam off-the-axis in such a way that it reaches the median plane (z = 0") with $p = p_z$ at the desired (x ≠ 0, y ≠ 0) point. For simplicity we have chosen the latter point as y = 0 x = 10 mm, i.e. with a 10 mm off-axis displacement. The same consideration would apply, of course, to any given (x,y) point.

The equations of motion in the presence of electric and magnetic fields, are reported in App. (B), together with their linearized expression which is, to first order,

quite sufficient. It is easy to see from eq. (B8) of App. (B) that in order to have a certain set of x and y values, and $p_x = p_y = 0$, at z = 0", four independent deflecting fields, Ex_1, Ex_2, and Ey_1, Ey_2 are necessary. Although the calculations reported here have been checked rigorously by integrating the non-linear set (B3), the use of the linearized equations gives a good starting point.

A sketch of a possible deflector geometry is shown in Fig. 9. Two sets of parallel plates give, for each deflector, an independent E_x, E_y control. Uniformity of the fields on the spatial range needed by the beam has been checked with TRIM, and found out to be better than 1%-2%, which we consider acceptable.

Should more detailed studies prove that this is not the case, they could obviously be substituted with four more conventional deflectors, each one consisting of a single set of parallel plates.

The results of center-ray tracking through this system are shown in Fig. 10, all the details being given in a straightforward way on the figure itself. The trajectory, for a q/A=0.5 ion, and 20 kV injection voltage, is on the magnet axis up to the deflectors, which are located just before the plug. It is bent afterwards in such a way as to reach the median plane off-axis in the required position. The vector radii of the trajectory, connecting its points to the z-axis, are also shown in order to clarify the spatial behavior. More detailed examples will be discussed, for the final geometry, in Sect. 4.
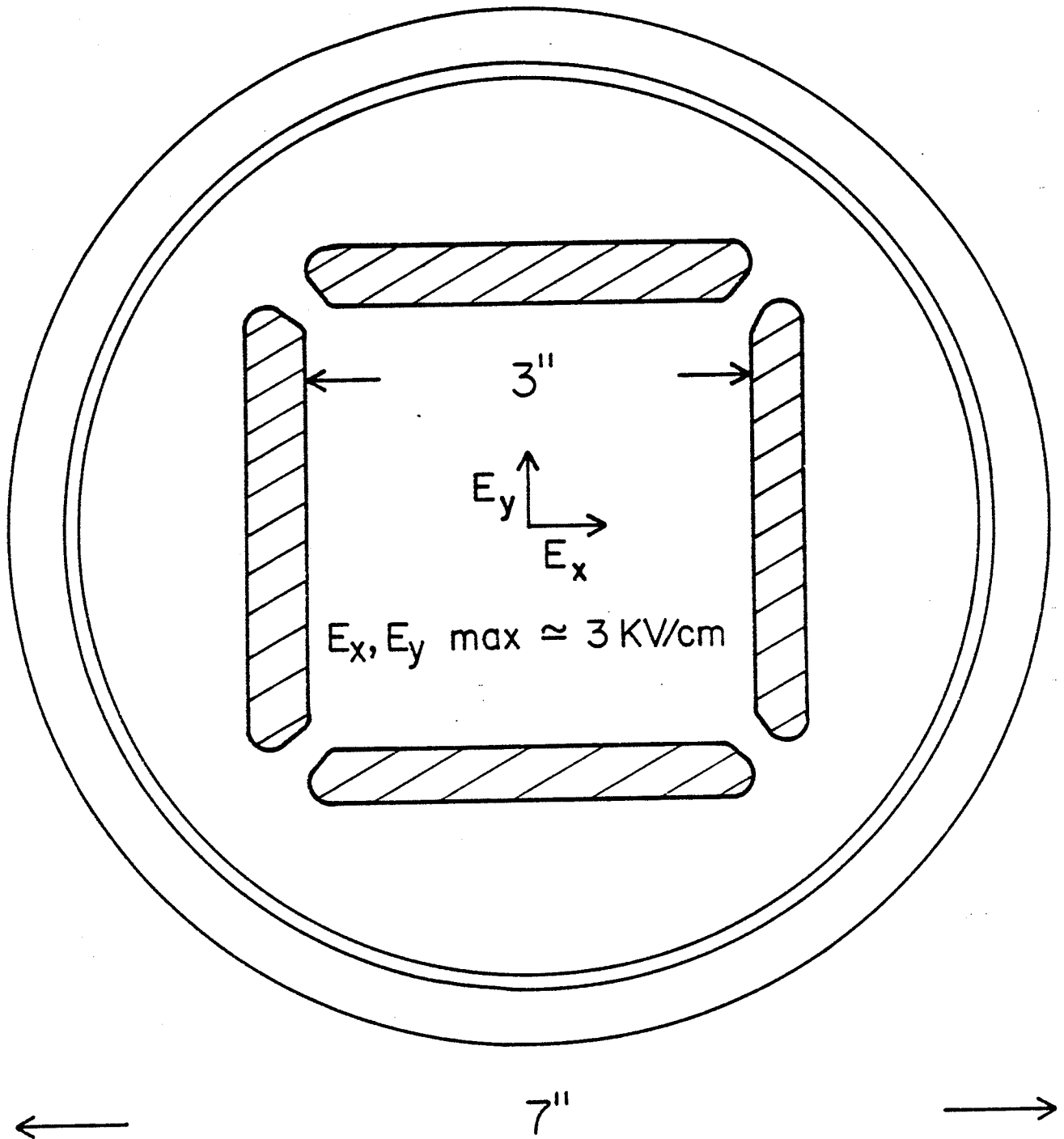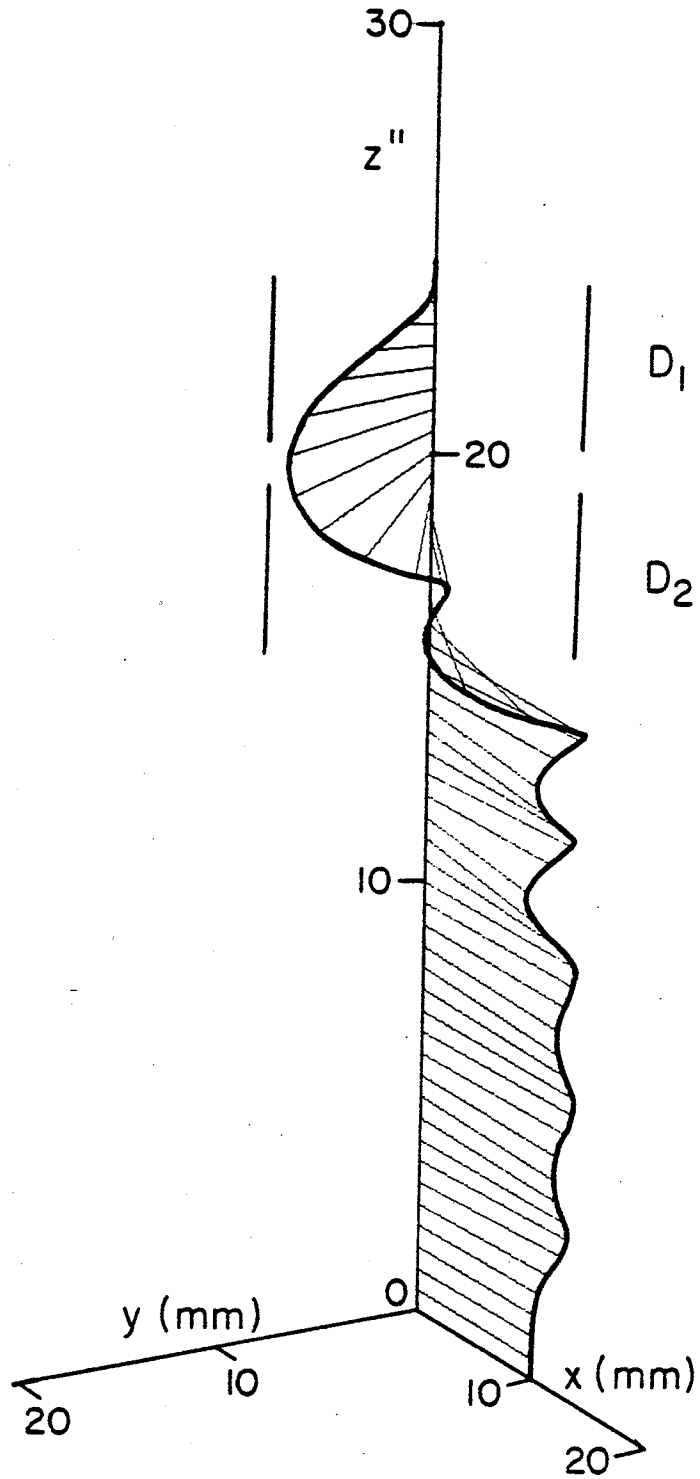
FIG. 9. Sketch of a possible deflecting plates geometry.

$$q/A = 0.5, \ 10 \ keV/n$$

$$B_0 = 34.6 \ kgauss$$

FIG. 10. Center ray trajectory through the deflectors with a 10 mm off-axis displacement.

Having thus ensured the possibility of injecting off-the-axis, the question remains as to whether the plug itself should also be off the magnet axis, or not. The first option obviously introduces a disturbing first harmonic on the magnetic field, which could be compensated but at the cost of a higher mechanical complexity.

Phase space tracking allows a selection between the two different options. This is shown in Fig. 11. Uncoupled and symmetric (x,p_x) and (y,p_y) phase spaces are tracked backwards from the median plane: in the (x,p_x) plane we represent both the phase space figures directly associated to the (x,p_x) coordinates (solid line) and those deriving from the (y,p_y) phase space (dashed line) via the magnetic field coupling which generates a rotation around the axis. The results are shown at different distances z from the median plane.

The beam on-axis, plug on-axis configuration (bottom strip), corresponds to on-axis injection and should be assumed as a reference in the sense that phase space distortions cannot be smaller. Some severe distortions are indeed observed in the beam off-axis, plug on-axis case, top strip. However, the presence of similar distortions also in the beam off-axis, plug off-axis case, middle strip, led us to analyze in more detail their causes. It was found that it is the sharp field gradients produced by the plug which are mostly responsible for their appearance, and the plug geometry had therefore to be optimized for this purpose.
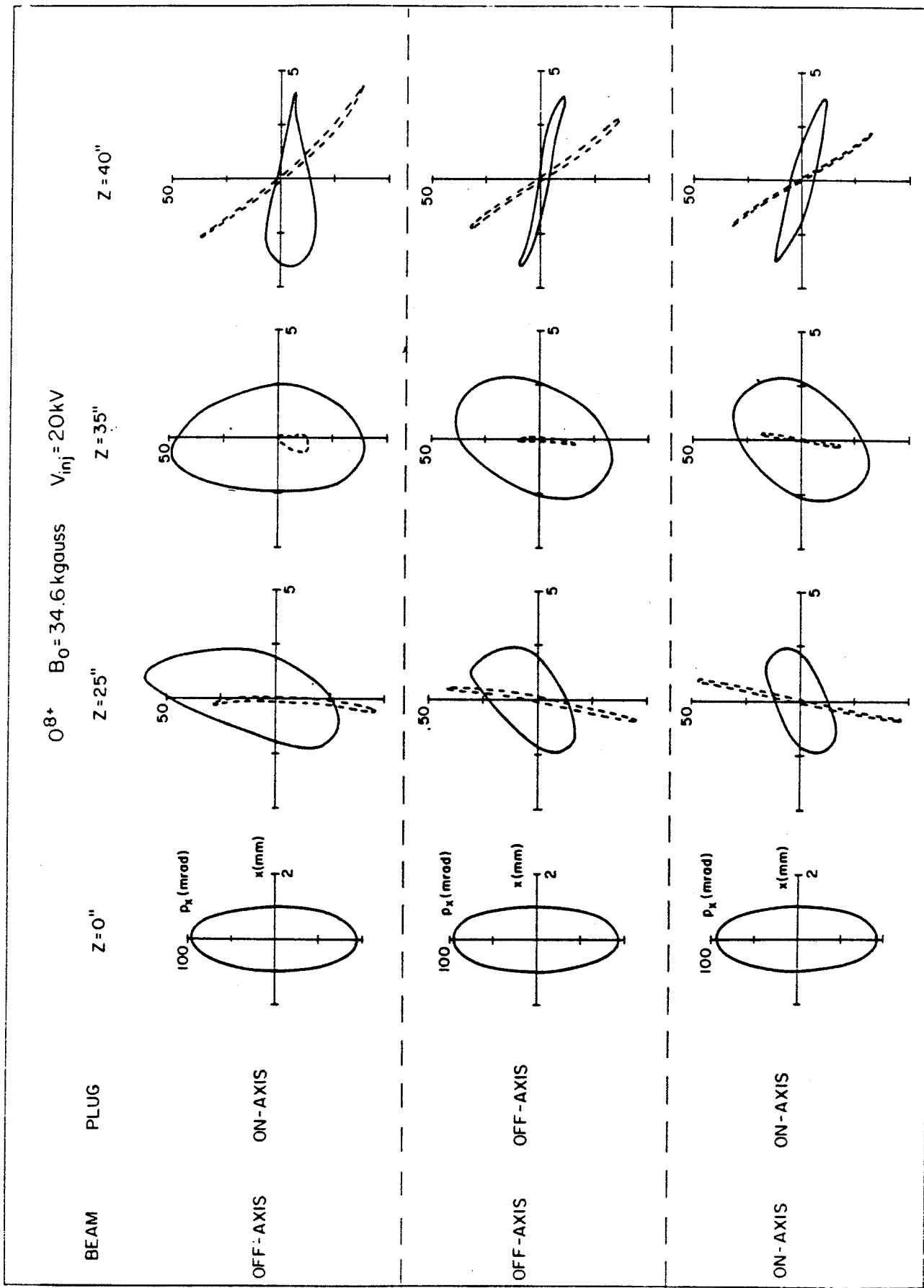
12

FIG. 11. Phase space plots at four different distances from the median plane for the q/A = 0.5 ion and 10 keV/n. Three combinations of center plug and injection trajectory positions with respect to the magnet axis are considered (see text for details).

3.3 Plug geometry optimization

Tapered plug geometries have been tried in order to reduce the field gradient at the plug entrance. An example is shown in Fig. 12, at the excitation needed for the q/A=0.5 ion, at B_o = 34.6 kGauss. As quite evident, and contrary to what intuition would suggest, it is the plug no. 2, i.e. with a reverse tapering, that has a beneficial effect on said gradient. This indicates that the latter is actually due to magnetic field lines from the larger hole concentrating on the plug entrance. Consequently the plug should be long enough as to terminate in a region where the B_z magnetic field is sensibly lower.

A plug extending up to 18" from the median plane produces the field shown in Fig. 13, the coil excitations being the same of Fig. 12. The gradient is indeed quite reduced, and by suitable tapering one could obtain even the curve labelled "smoothed". It has been checked, however, that at these very reduced gradients no sensible differences exist between the phase spaces if either of the two fields is used.

Consequently the long plug has been selected. The field along the hole at the excitation needed for the U^{46+}, at B_o = 47.5 kgauss is shown in Fig. 14. In this case also the gradient at the plug entrance is quite reduced, as can be seen by comparing with Fig. 7.

The deflectors needed to perform the off-axis injection are therefore located before the plug entrance and are 4"
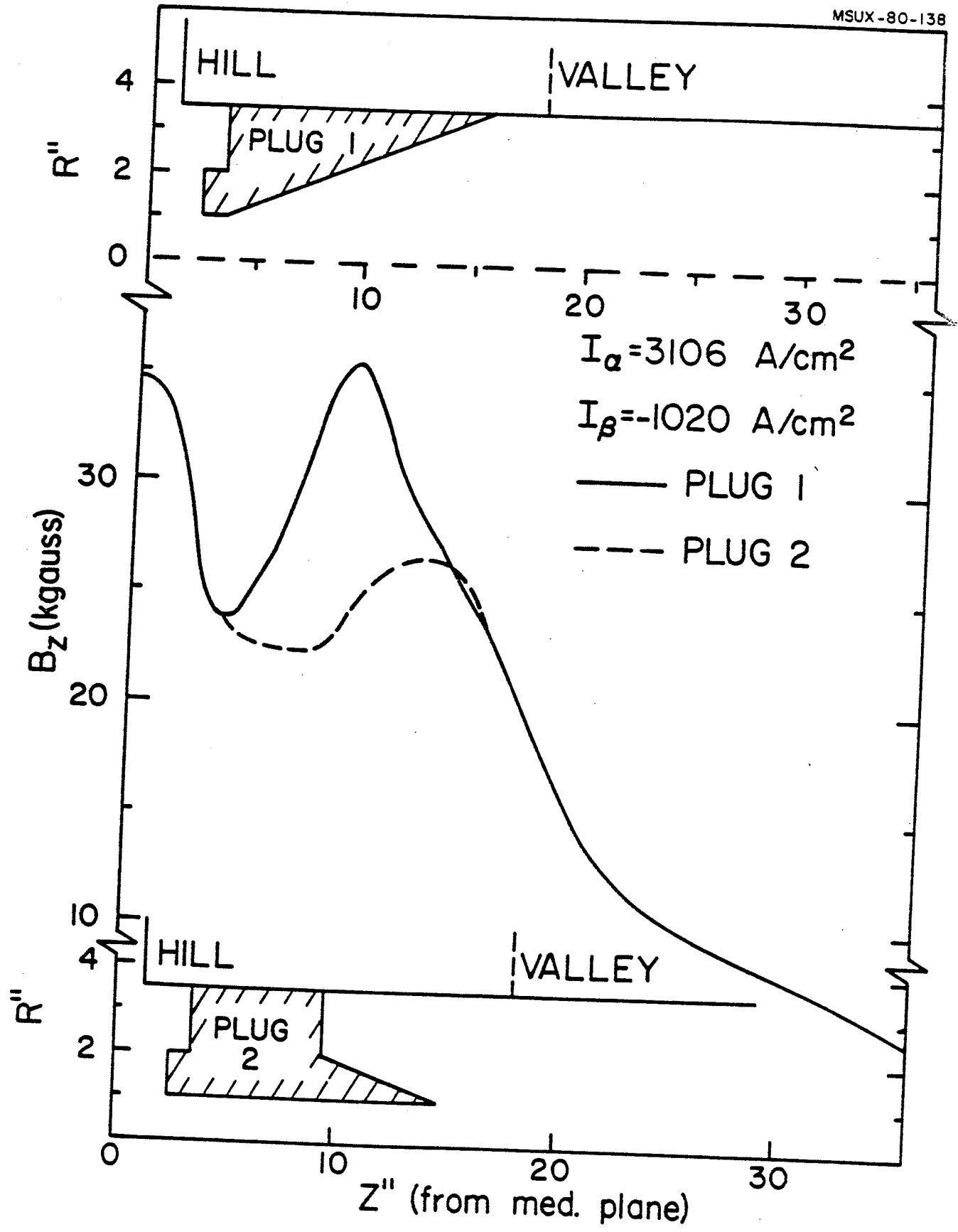
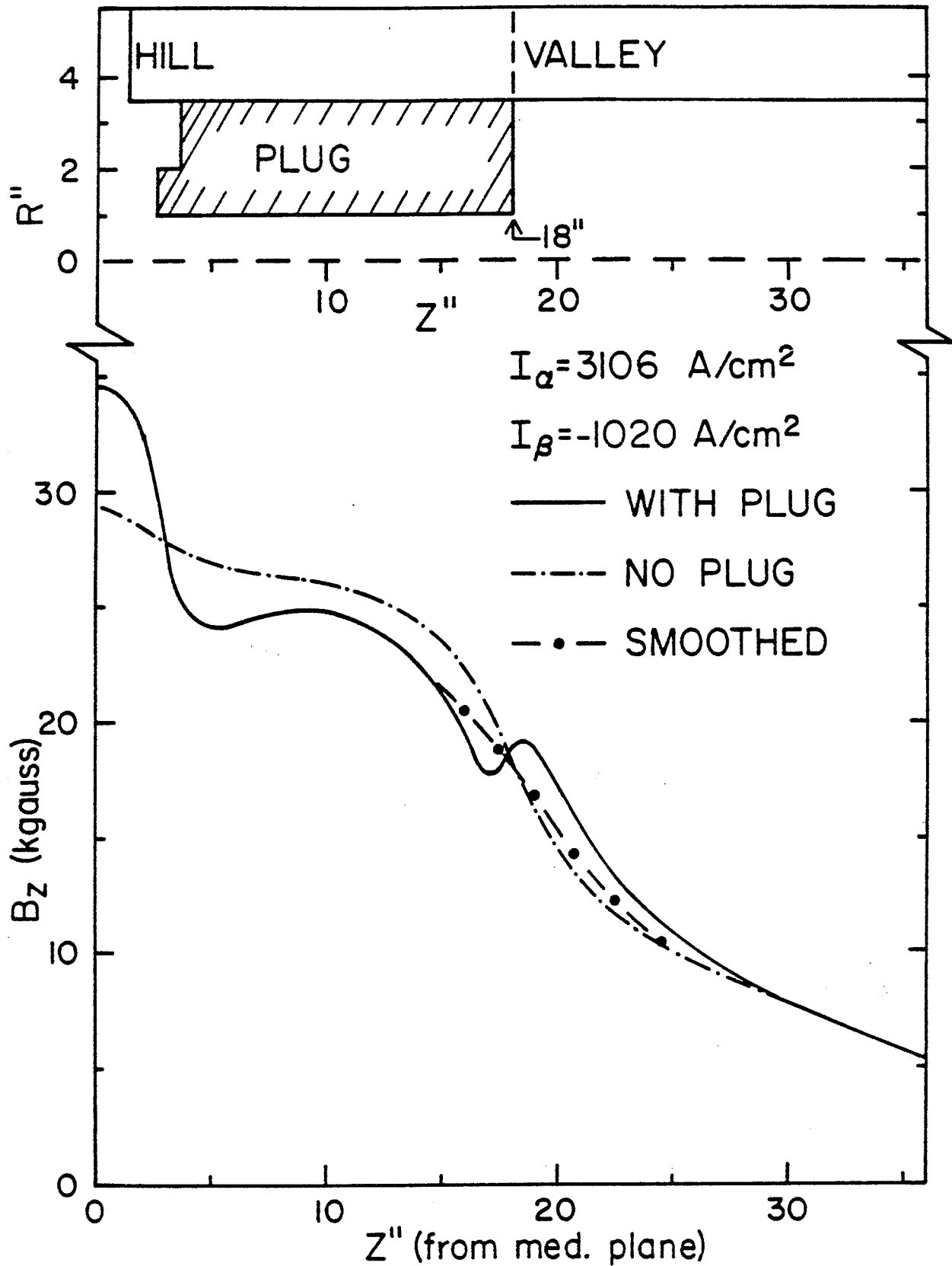FIG. 12. Magnetic field along the hole axis for the two different center plug geometries shown.

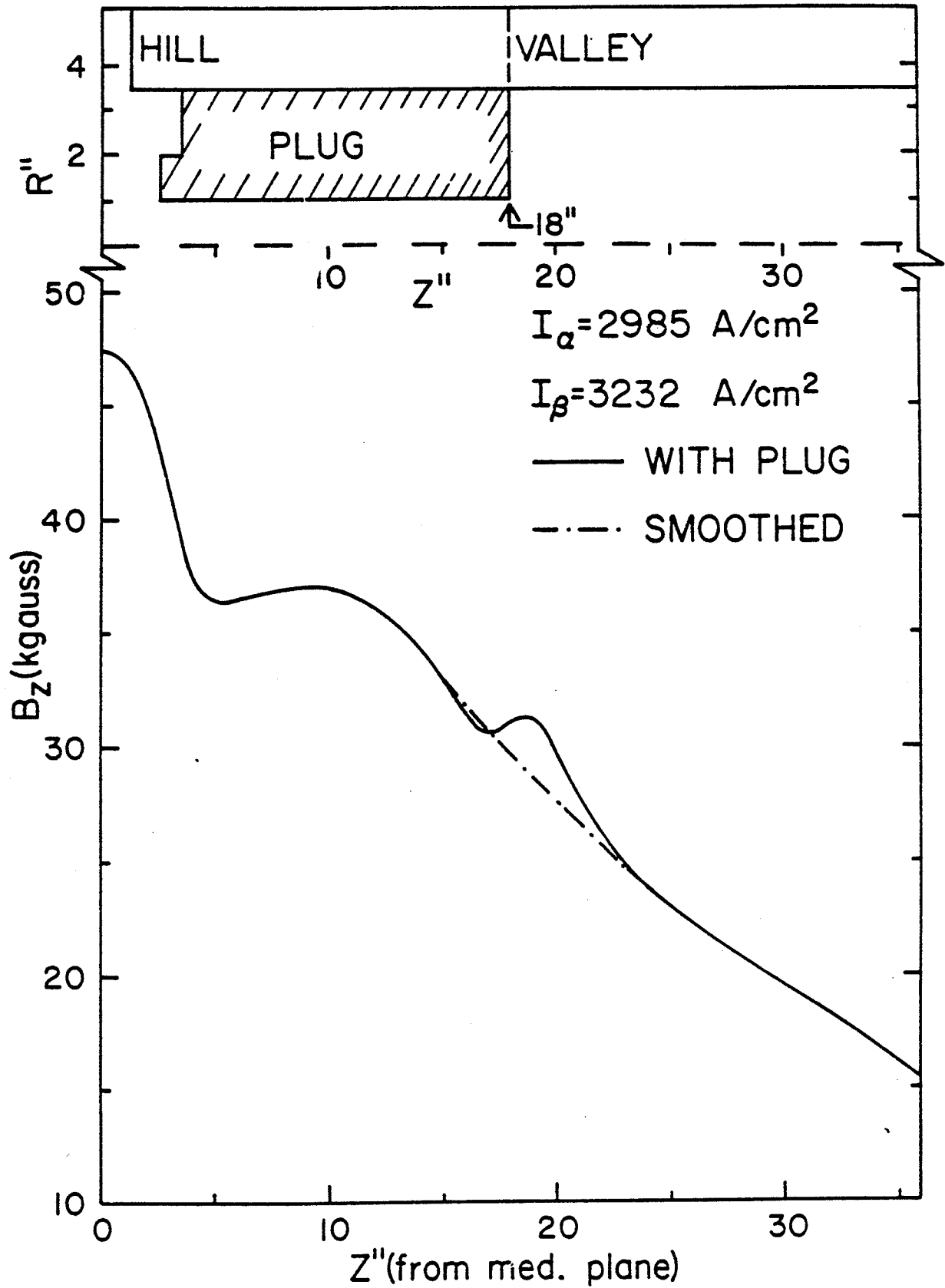FIG. 13. Magnetic field along the hole axis for the center plug geometry shown at the top.

FIG. 14. Magnetic field along the hole axis for the center plug geometry shown at the top. Coil excitations correspond to the U^{46+} ion, B_o = 47.5 kG.

long. The first set is located between 20" and 24" from the median plane, and the second between 25"-29".

The center ray trajectories are shown, for the two representative ions, in Fig. 15, other details being given on the figure itself. In order to better visualize the spatial extent of the trajectories, their projections on the (z,x) plane and (x,y) plane are presented in Fig. 16. In order to inject at 10 mm off-axis in the x direction, the ray must go about 12 mm off axis in the y-direction as well as 15 mm off axis in he x-direction. This takes place essentially in the deflectors, as can be judged by the (z,x) projections, and therefore these numbers define the minimum spatial extent of the deflectors themselves.

With this optimized plug design, phase space tracking shows no sensible differences between the cases where the beam is injected along the axis or off the axis. This is shown in Fig. 17 for the q/A=.5 ion, where the top and bottom strips can be compared at every distance from the median plane. A somewhat larger distortion is observed in the case of the U^{46+}, Fig. 18, but it is also seen that the phase space recovers after z = 35", i.e. after the deflectors are traversed.

As a consequence we have chosen to study the phase space matching problem with the geometry just discussed, assuming that no off-axis displacement of the plug will be necessary. This choice eliminates problems of first

MSUX-80-321

O^{8+} $B_0 = 34.6$ kgauss $V_{inj} = 20$ kV

DEFL.	POS.	E_x(kV/cm)	E_y(kV/cm)
1	25"-29"	-.983	-.485
2	20"-24"	1.255	-2.285

U^{46+} $B_0 = 47.5$ kgauss $V_{inj} = 15$ kV

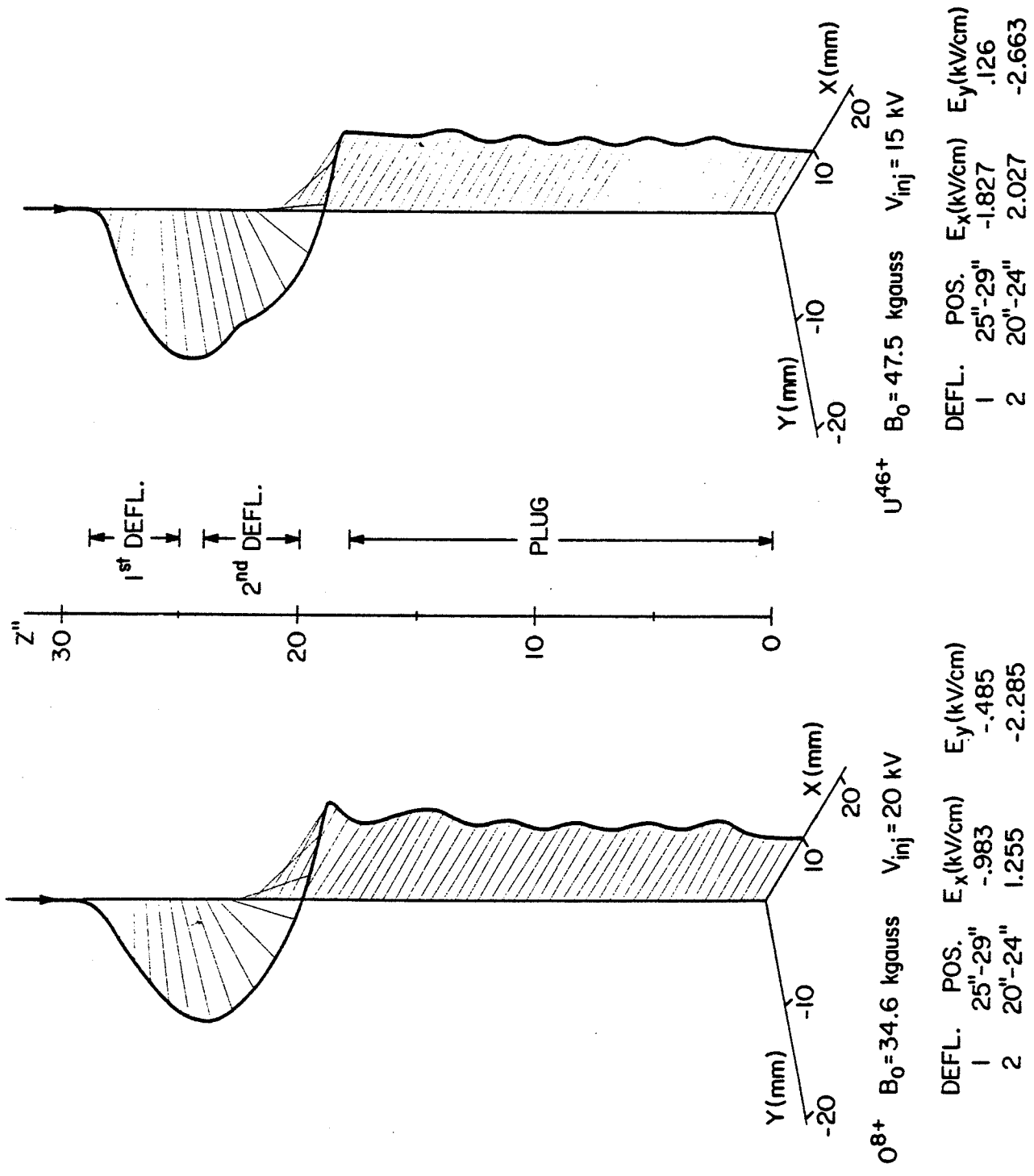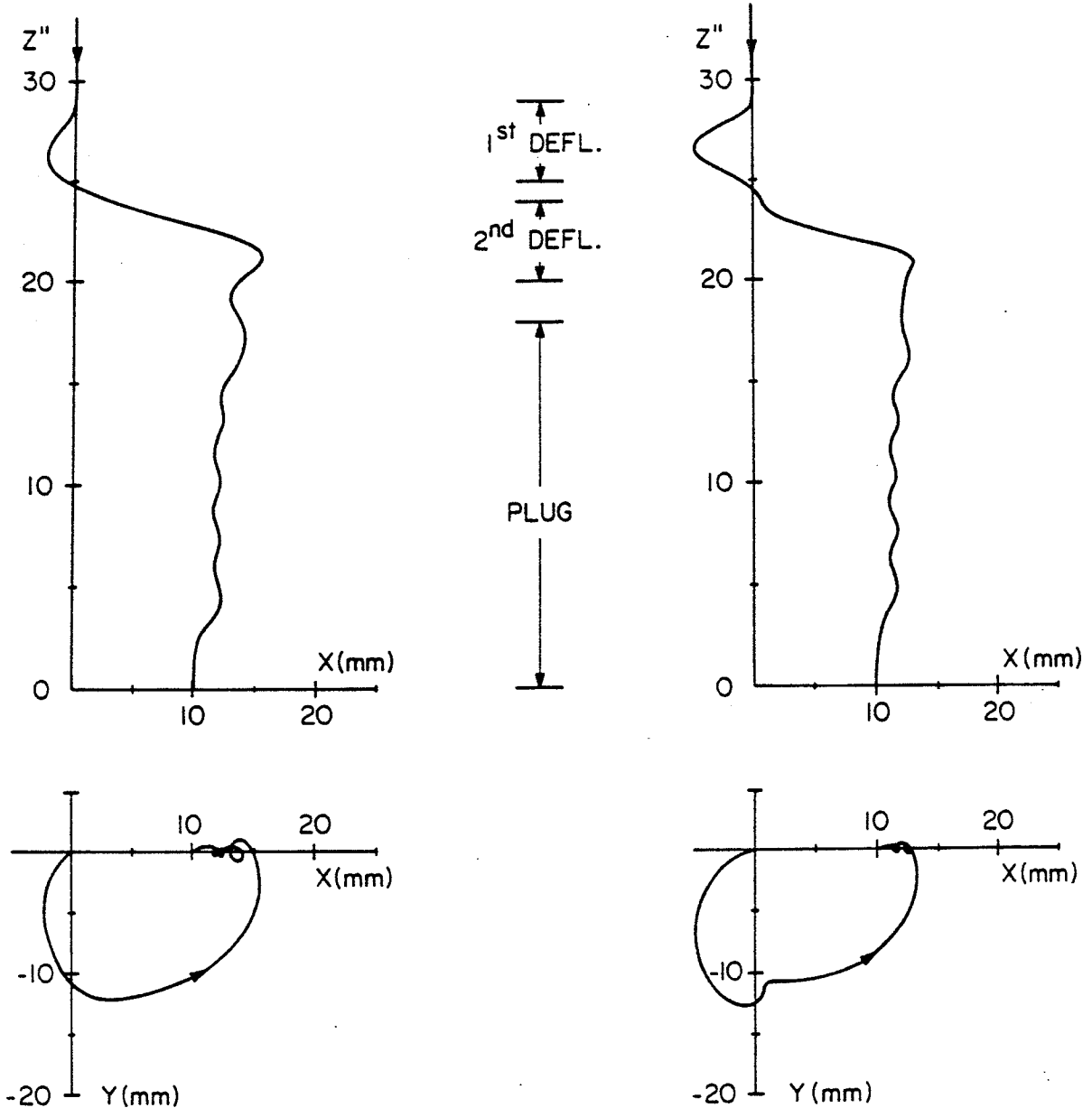| DEFL.	POS.	E_x(kV/cm)	E_y(kV/cm)
1	25"-29"	-1.827	.126
2	20"-24"	2.027	-2.663

FIG. 15. Center ray trajectories for the field with the plug extending up to 18 inches from the median plane. The O^{8+} ion at 10 keV/n and the U^{46+} ion at 2.9 keV/n are shown.

O^{8+} $B_0 = 34.6$ kgauss $V_{inj} = 20$ kV

U^{46+} $\dot{B}_0 = 47.5$ kgauss $V_{inj} = 15$ kV

DEFL	POS.	E_x(kV/cm)	E_y(kV/cm)
1	25"-29"	-.983	-.485
2	20"-24"	1.255	-2.285

DEFL	POS.	E_x(kV/cm)	E_y(kV/cm)
1	25"-29"	-1.827	.126
2	20"-24"	2.027	-2.663

FIG. 16. Projections of the center ray trajectories of Fig. 15 into the (x,z) and (x,y) planes.
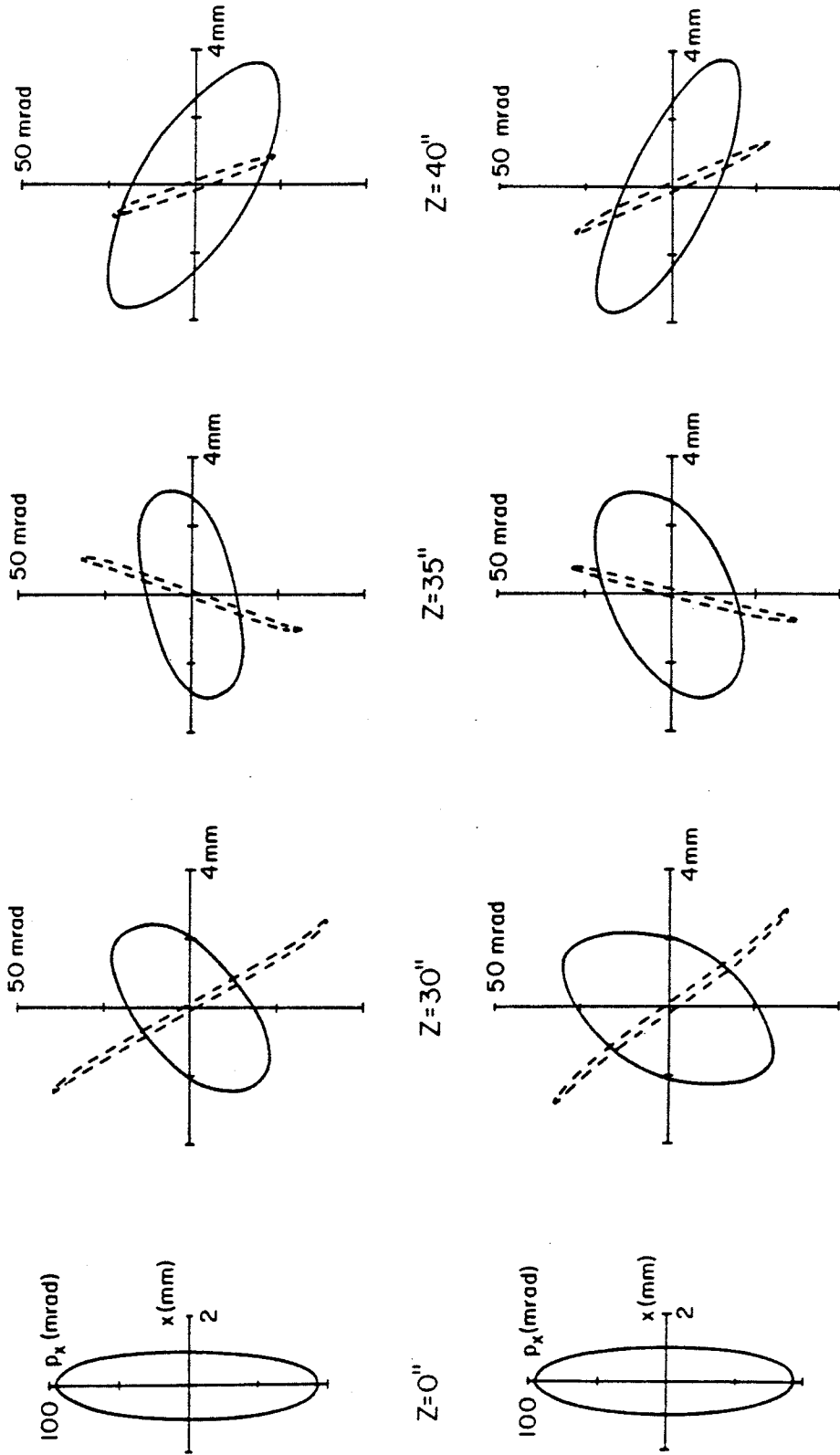
FIG. 17. Phase space plots at the median plane (z=0) and at three different positions along the axis. Both, beam on-axis (top), and beam off-axis (bottom) cases are shown for the q/A = 0.5 ion. In the latter case the beam is back on axis at z = 29 inches. Deflector distances from the median plane are also indicated.
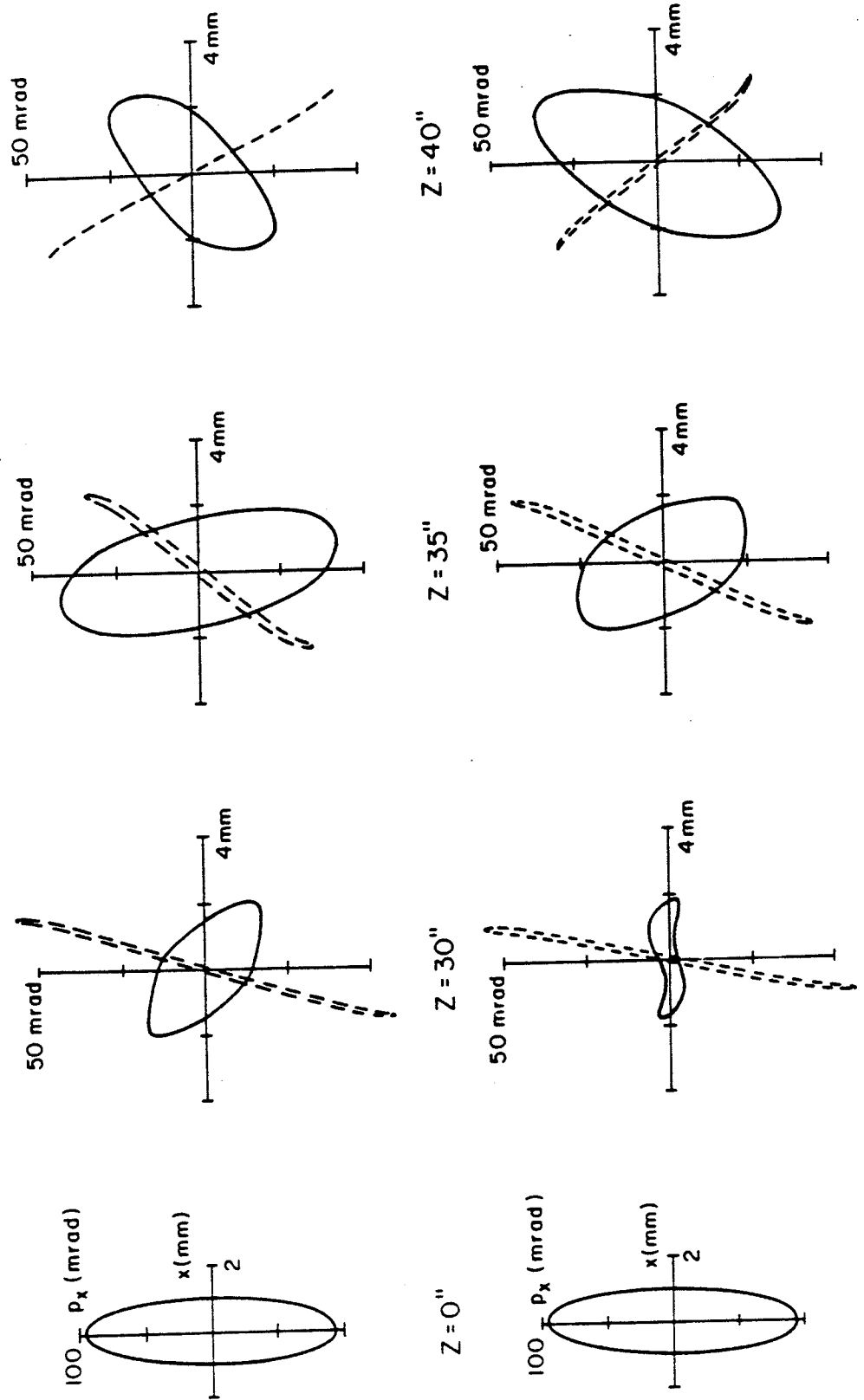
FIG. 18. Similar to Fig. 17, but for the U^46+ ion.

harmonic correction, and makes the field geometry independent
of the center region geometry, i.e. the optimum position
of the mirror for centering purposes can be chosen without
affecting the magnetic field.

4. Beam transmission through the yoke

4.1 General considerations

In this section we investigate the problem of beam
transmission through the yoke, from the injection point
(I.P., at z = 100") down to the mirror entrance. The latter
practically coincides with the median plane. This problem
is obviously related to the more general question of phase
space matching between the external source and the cyclotron.
The latter topic deserves, however, a very careful and rigorous
analysis which must include also the inflection into the
median plane, and is carried out in Sec 5.

Presently we shall therefore limit ourselves to a dis-
cussion of the optical elements which can be used in order
to have a well-confined beam in the path through the yoke
bore. The calculations described below assume the following

-   a beam emittance, at I.P., of 300 mm mrad in both
    the (x,p_x) and (y,p_y) phase subspaces, assumed uncoupled.
    From the available data[15] it seems that emittances
    of 300-400 mm mrad in both transversal phase spaces
    at 10 keV/n are realistic for the mentioned ion sources,
    and fully stripped light ions. Since cyclotron accept-

ances are at least that large, a reference value of
300 mm-mrad has been assumed.

- double waist requirement, at the median plane, with
half-width of 1. mm, in both phase spaces.
- range of injection voltages, as discussed previously,
of $15 \leq V_{inj} \leq 25$ kV for the ion with q/A=0.5, and
$10 \leq V_{inj} \leq 20$ kV for the uranium ion.

These assumptions are made merely to exemplify the
beam behavior in the yoke transversal, under realistic cons-
traints. As already outlined in Sec. 3, a strong coupling
between the (x, p_x) and (y, P_y) phase spaces will take place
along the injection path, physically due to the rotation
of the ions around the z-axis. An increase in phase space
area can therefore be expected. However, as stated above,
we shall present here only the results from the point of
view of beam confinement, postponing a more complete dis-
cussion to Sec. 5.

That some optical elements will be needed along the
injection path just to confine the beam can be readily seen
from Fig. 19. In this figure the beam envelopes, traced
backwards from the median plane under the assumptions just
listed, are shown for both representative ions and three
selected injection voltages. The beam exhibits a tight
confinement, with characteristic oscillations in the envelope
amplitude, up to 30"-40". There, depending upon the ion,
the magnetic field is still 20-15 kgauss. The wavelength
of the oscillations, λ, increases as a function of z, as
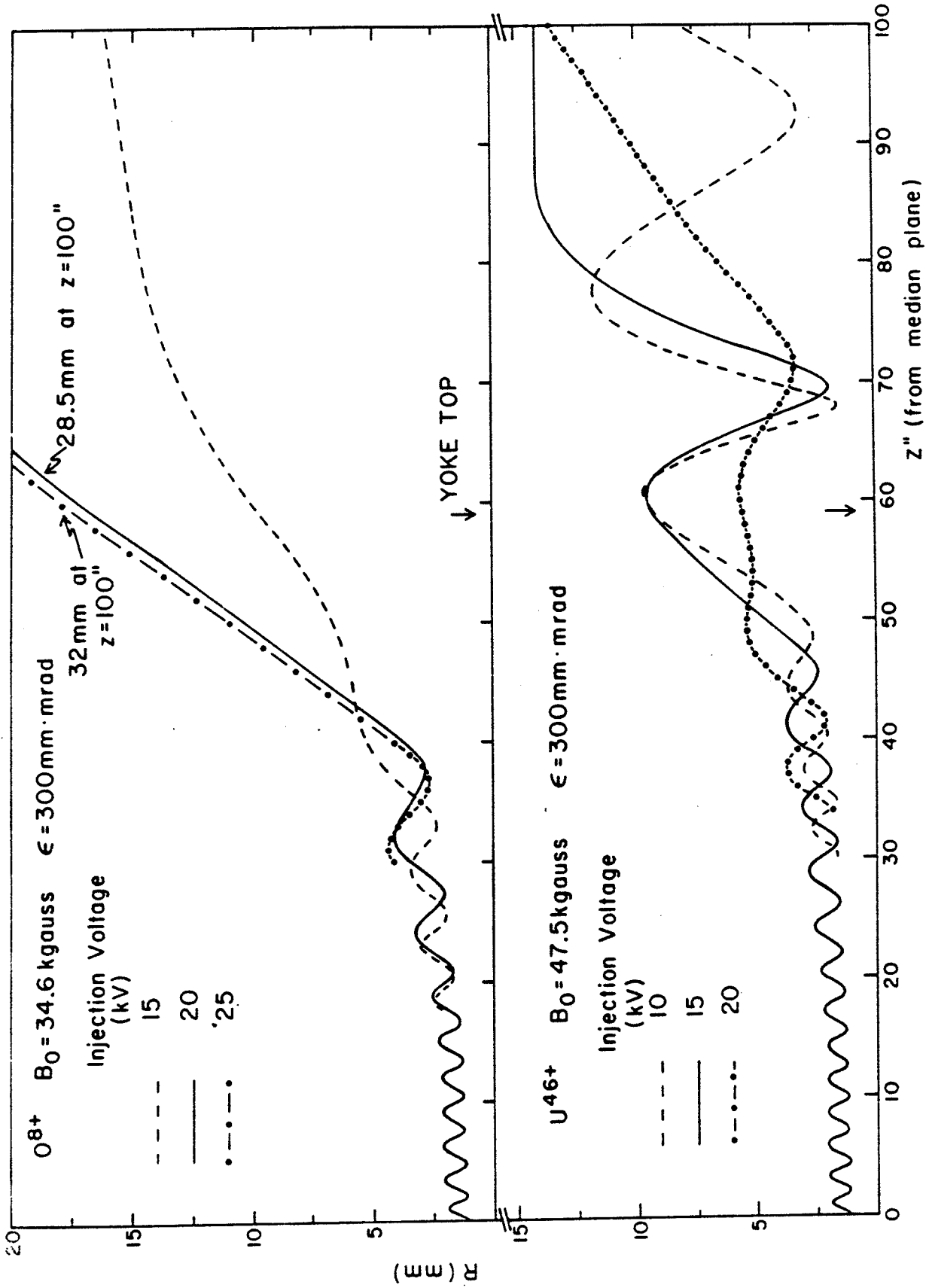expected from the formula

16

FIG. 19. Examples of beam envelopes for 300 mm·mrad beams, traced backwards from a waist (1 mm halfwidth) at the median plane.
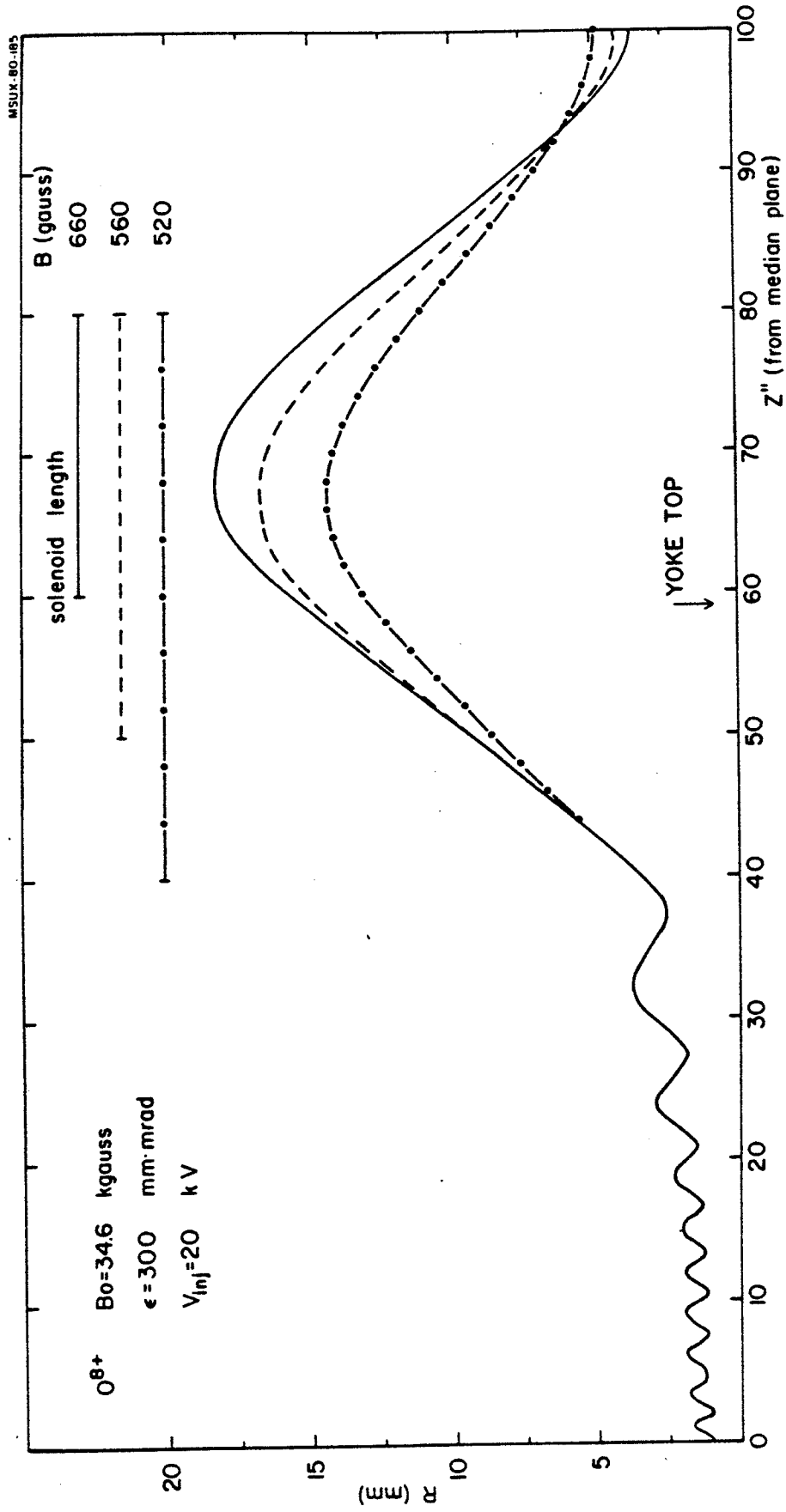
FIG. 20. Beam envelopes for the q/A = 0.5 ion traced
backward from a 1 mm halfwidth waist at the median plane.
The effect of three different solenoid lengths is shown.

$$B\lambda = 2\pi(B\rho)_{ion} \qquad\qquad (3)$$

As seen from the figure, the magnetic field in the hole is not by itself sufficient to keep the beam confined within acceptable limits up to the injection point at $z = 100"$, especially so in the case of the q/A=0.5 particle. This finding is independent of any requirement on phase space matching.

We have looked into three possibilities for achieving a satisfactory beam confinement:

- quadrupoles

- solenoids

- einzel-lenses.

The first one was quickly discarded, mainly because of the difficulty of predicting quadrupole strengths when the latter are immersed in a several kgauss longitudinal field. The tests we ran showed that the coupling between the two transversal phase spaces becomes rather involved and in any case simpler elements like solenoids or einzel-lenses proved more than adequate. We shall discuss first the results obtained with a solenoid.

4.2 Beam confinement with solenoids

Solenoids of various lengths produced, for the q/A=0.5 ion, the results shown in Fig. 20. As listed in the figure, the solenoid field is low, and corresponds roughly to one wavelength of envelope oscillation. The confinement effect

is sharp, the maximum beam halfwidth reaching about 17 mm, which is quite acceptable. Also, as can be appreciated from the envelope, the beam is very close to a waist at the injection point. The differences in beam amplitude between the three cases do not warrant however, in our view, the choice of a solenoid longer than the shortest one shown, which extends between 60" and 80" distance from the median plane.

The reason of choosing the latter is that in the case of the K-800 cyclotron the solenoid is fully outside the yoke, which reduces considerably any mechanical problem for its construction.

If the magnetic field in the solenoid is increased to produce two or three wavelengths oscillations, Fig. 21, no sizable advantages are gained in terms of beam confinement. The beam size is more or less the same at the injection point, as expected from elementary arguments, while the field has to reach the few kgauss level.

The short solenoid with the minimum field required for one full oscillation looks therefore the best choice. When checked as a function of the injection voltage, Fig. 22, the beam is still well confined. It should be remarked that the fields listed in the figure itself do not, and cannot, scale according to the particle energy because of the additional requirement that we have a waist, or close to it, at the injection point. This in order to simplify, whenever possible, matching problems.
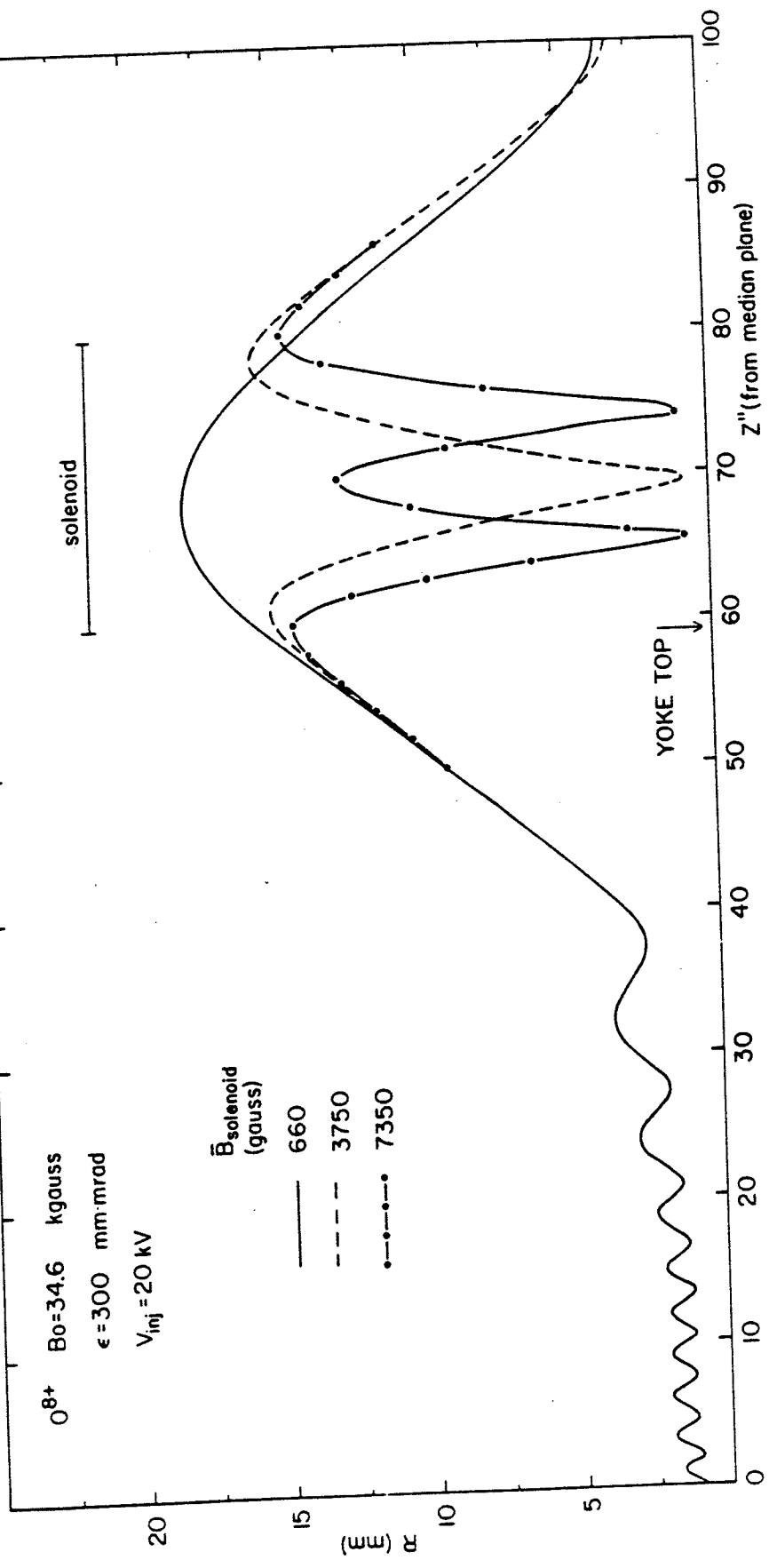
FIG. 21. Beam envelopes for the Q/A = 0.5 ion traced backward from a 1 mm halfwidth waist at the median plane. The effect of three different magnetic fields for the solenoid is shown.
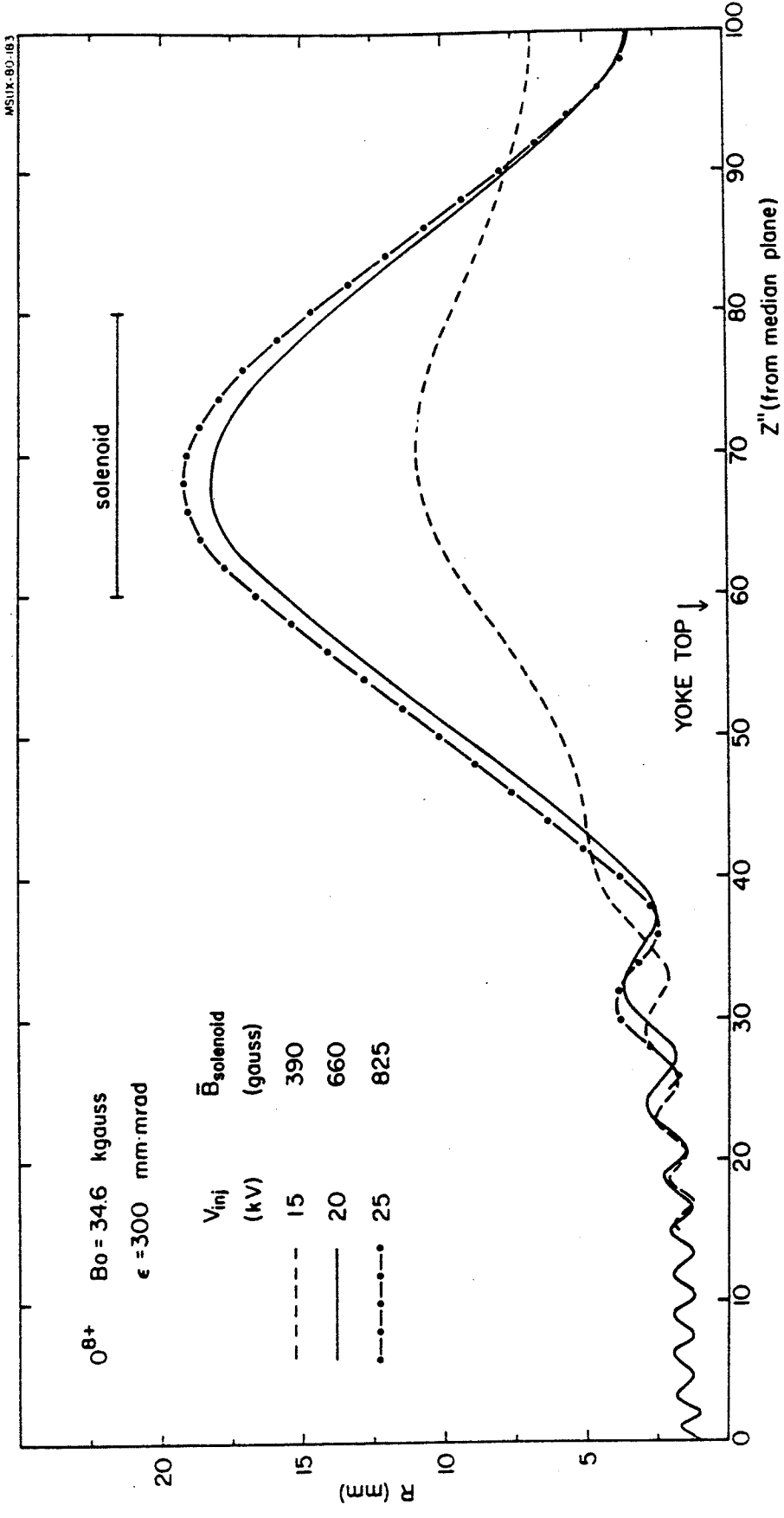
FIG. 22. Beam envelopes for the q/A = 0.5 ion at three
different inejction voltages. The magnetic field in the
solenoid is adjusted to produce one wavelength oscillation.

In fact, as can be seen in Fig. 23, in the proximity of $\lambda = 1$ one can vary the field around that required for the waist condition at the injection point (solid line), if for matching purposes one prefers to have a converging beam (dot-dash line), or a diverging one, (dashed line). In any case the solenoid keeps the beam confined at about the same width.

The envelopes for the case of the uranium ion, at the three selected injection voltages, are shown in Fig. 24. The beam confinement is obviously much better, because of the large intrinsic field in the hole, but the other characteristics remain qualitatively the same.

Turning now to a preliminary analysis of the phase space behavior for the central cases, i.e. $q/A=.5$ at $V_{inj}=20$ kV and $q/A=.19$ at $V_{inj}=15$ kV, it is shown in Fig. 25 both at the injection point and at the median plane. They correspond strictly to the envelopes discussed previously, all details being given in the figure itself.

Here, as in all similar figures reported later, only the (x,p_x) space is presented, the beam being symmetric in the two transversal subspaces. The solid line corresponds to the total phase space, which includes coupling, the dashed one to the (x,p_x) component, the dotted one to the (y,p_y) component showing up in the (x,p_x) plane because of the coupling.

We observe indeed an emittance increase due to the coupling, which in this particular case is rather limited.

MSUX-80-175

O^{8+} $B_0 = 34.6$ kgauss

$\epsilon = 300$ mm·mrad

$V_{inj} = 20$ kV

$\bar{B}_{solenoid}$

- - - - -   505

————   660

—·—·—   795

solenoid

R (mm)

Z" (from median plane)
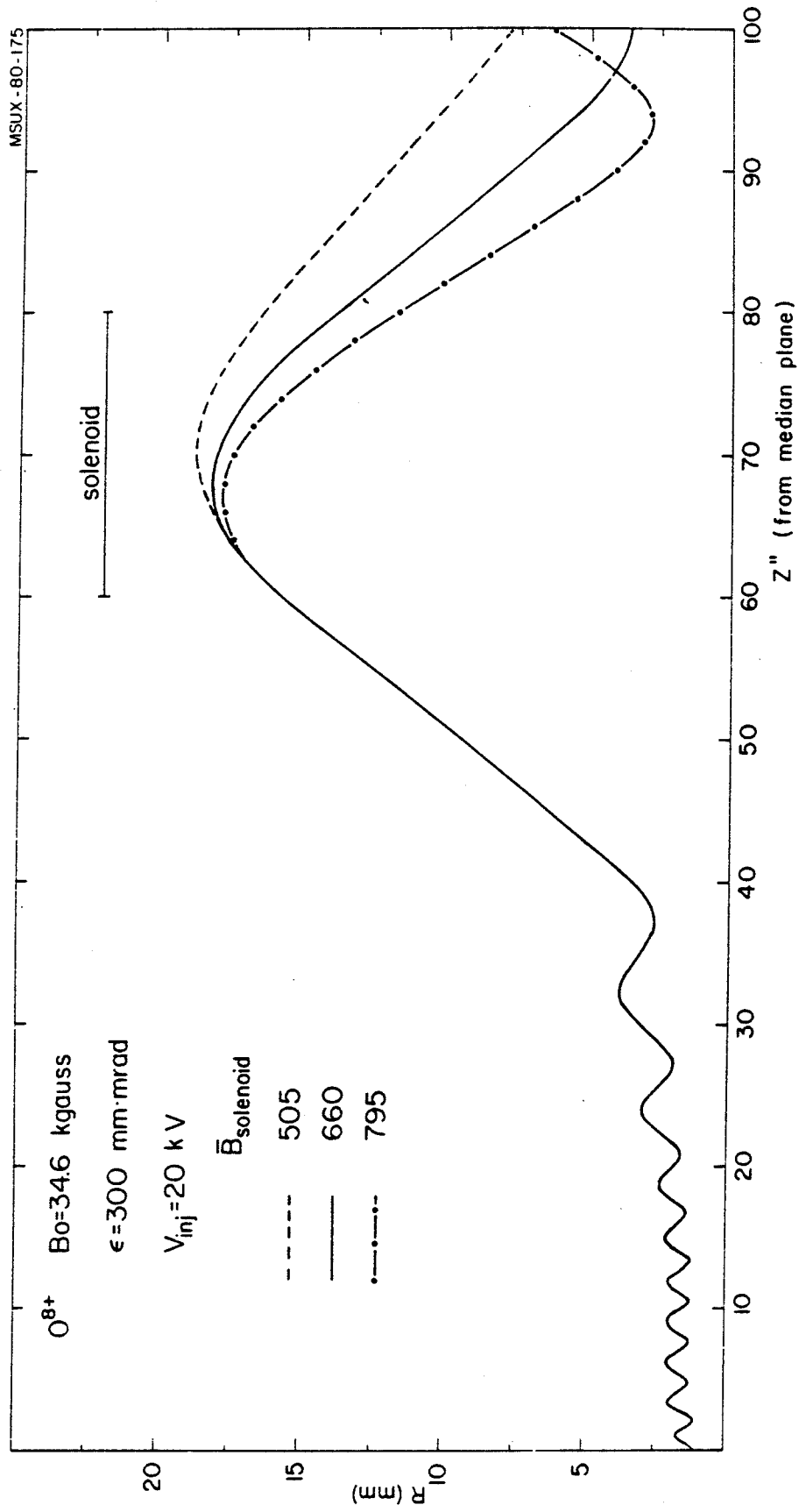
FIG. 23.   Beam envelopes for the Q/A = 0.5 ion at a fixed injection voltage of 20 kV. The effect of varying the solenoid field is shown.

U^{46+} Bo=47.5 kgauss

ϵ=300 mm·mrad

V_{inj} (kV)	$\bar{B}_{solenoid}$ (gauss)
10	-345
15	725
20	1450

solenoid

YOKE TOP

R (mm)

Z" (from median plane)

FIG. 24. Similar to Fig. 22 but for the U^{46+} beams.

FIG. 25. Phase space behaviour of the two representative ions at the median plane (waist) and at the injection point (see text for details).

At the median plane a waist of the required dimensions is nevertheless obtained.

The phase spaces for different injection voltages are shown for both ions in Figs. 26 and 27 respectively. The features just discussed above can be easily recognized. It will be noted that only in the case of the uranium ion with 20 kV injection voltage we are unable to start with a waist also at the injection point ($z = 100"$), but we need there a converging beam. This beam, as well as the waists needed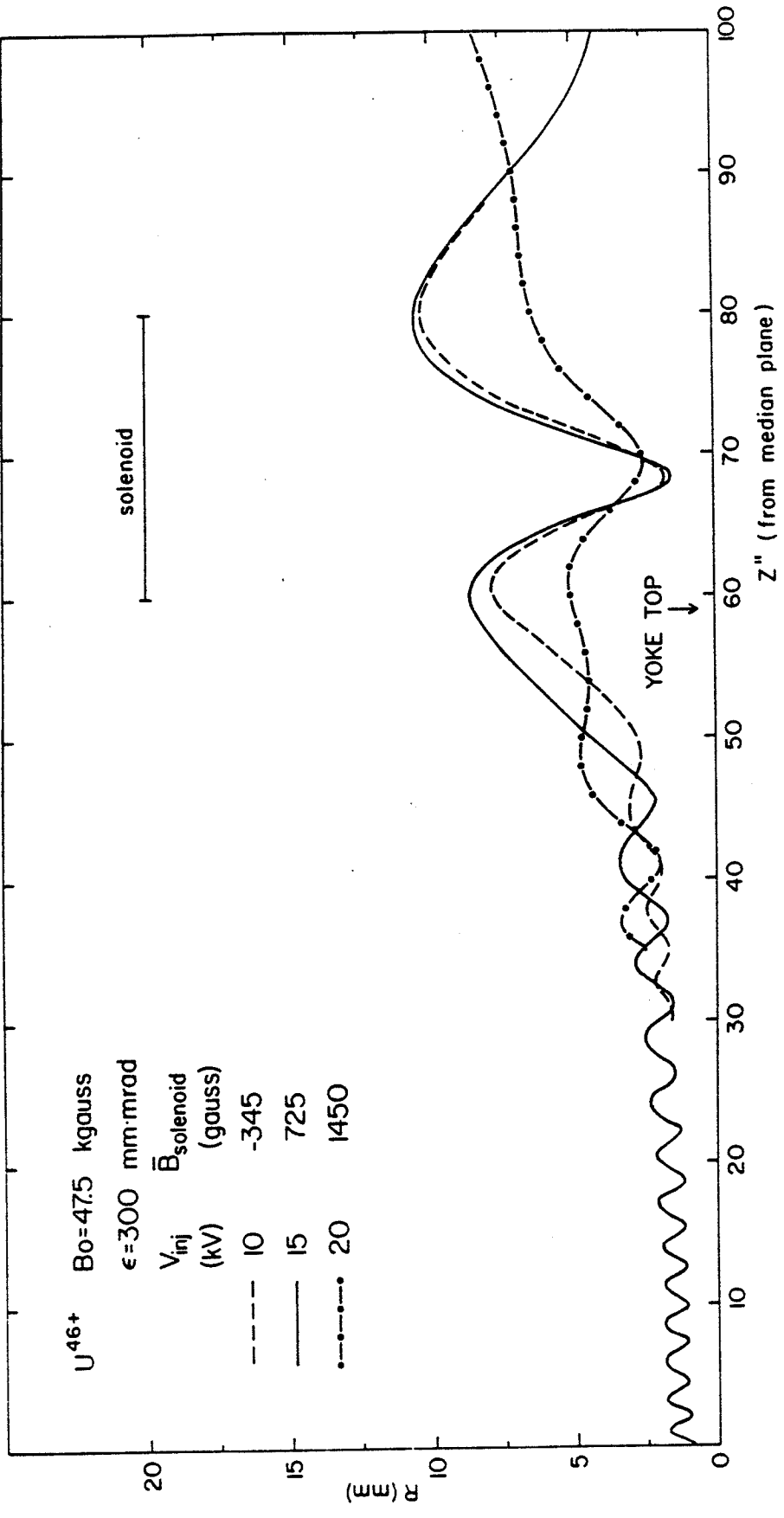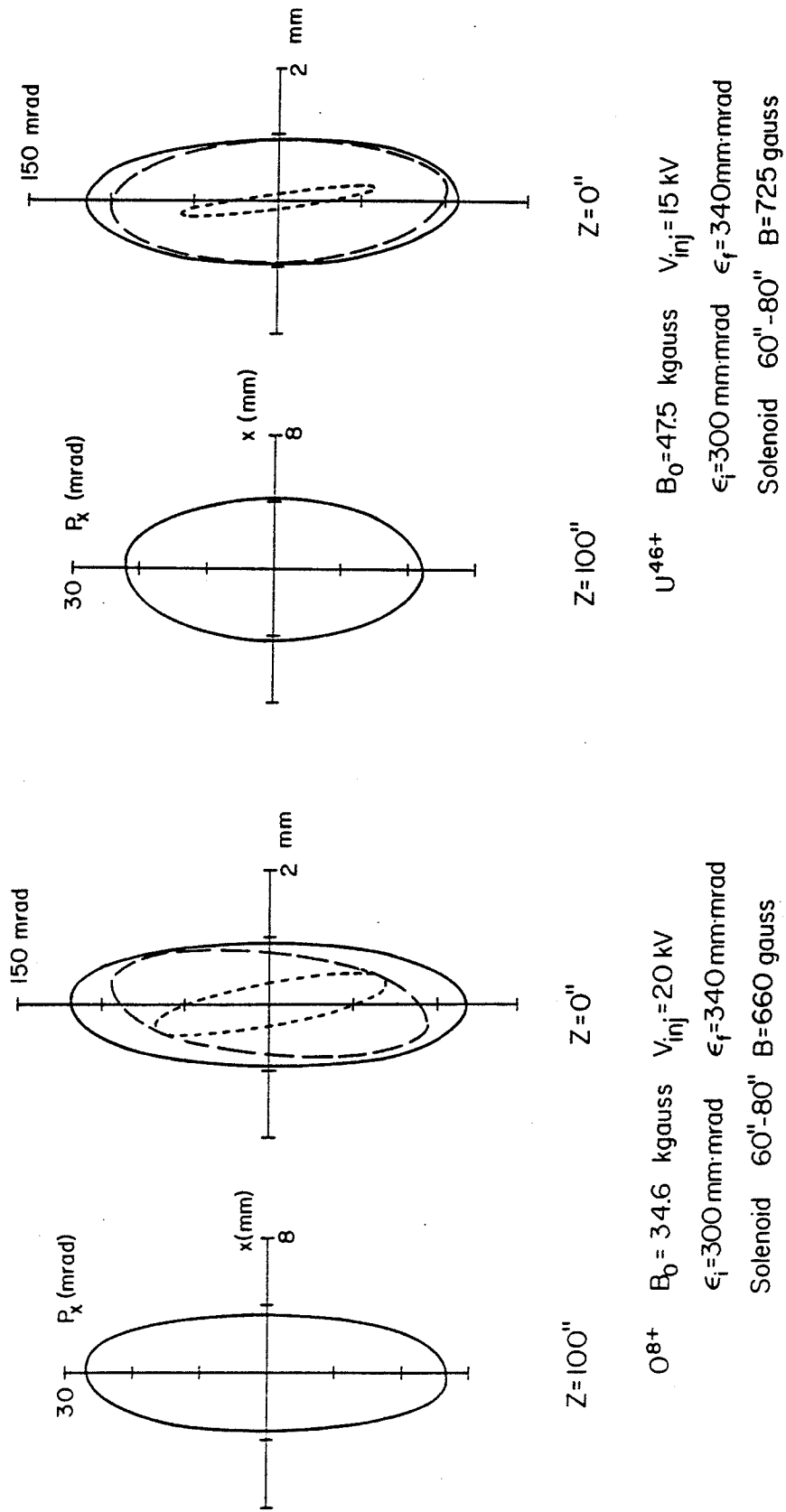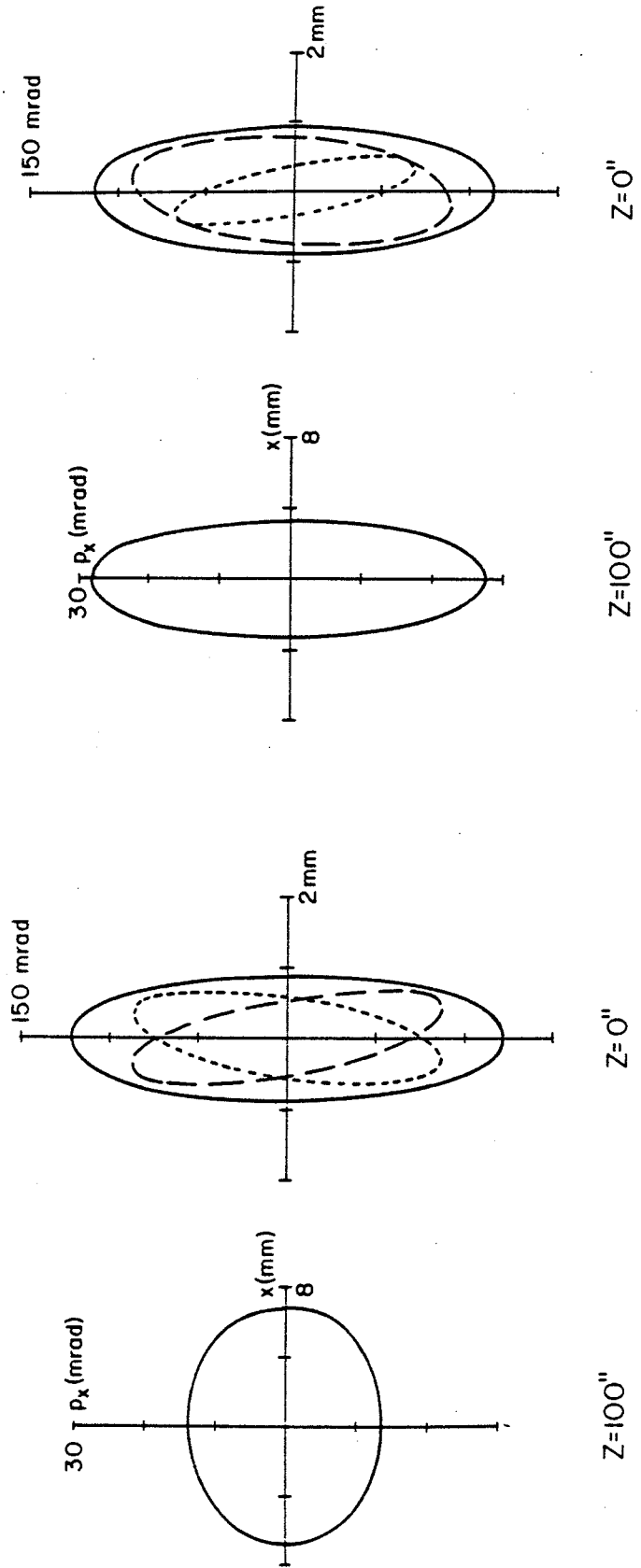 in all other cases, should however be easy to produce with any transmission line between the ion source and the injection point.

As a summary, the single solenoid, 20" long, and with magnetic fields not exceeding 1-1.5 kgauss seems a rather good solution to the beam confinement problem. Given the low field, this solenoid could be either superconductive or conventional, although the superconducting solution with a cold bore is in our view more attractive.

4.3 Beam confinement with einzel lenses

The use of einzel lenses has also been investigated under the same assumptions, although not in as much detail.

We have found that two einzel lenses are necessary for the $q/A=0.5$ ion, while only one is needed for the uranium case, due to the higher intrinsic beam confinement. The beam envelopes are shown for both ions in Fig. 28, where also the lenses positions and voltages are given. A voltage

20

FIG. 26. Phase space behaviour of the q/A = 0.5 ion for two different injection voltages, at the median plane and at the injection point.
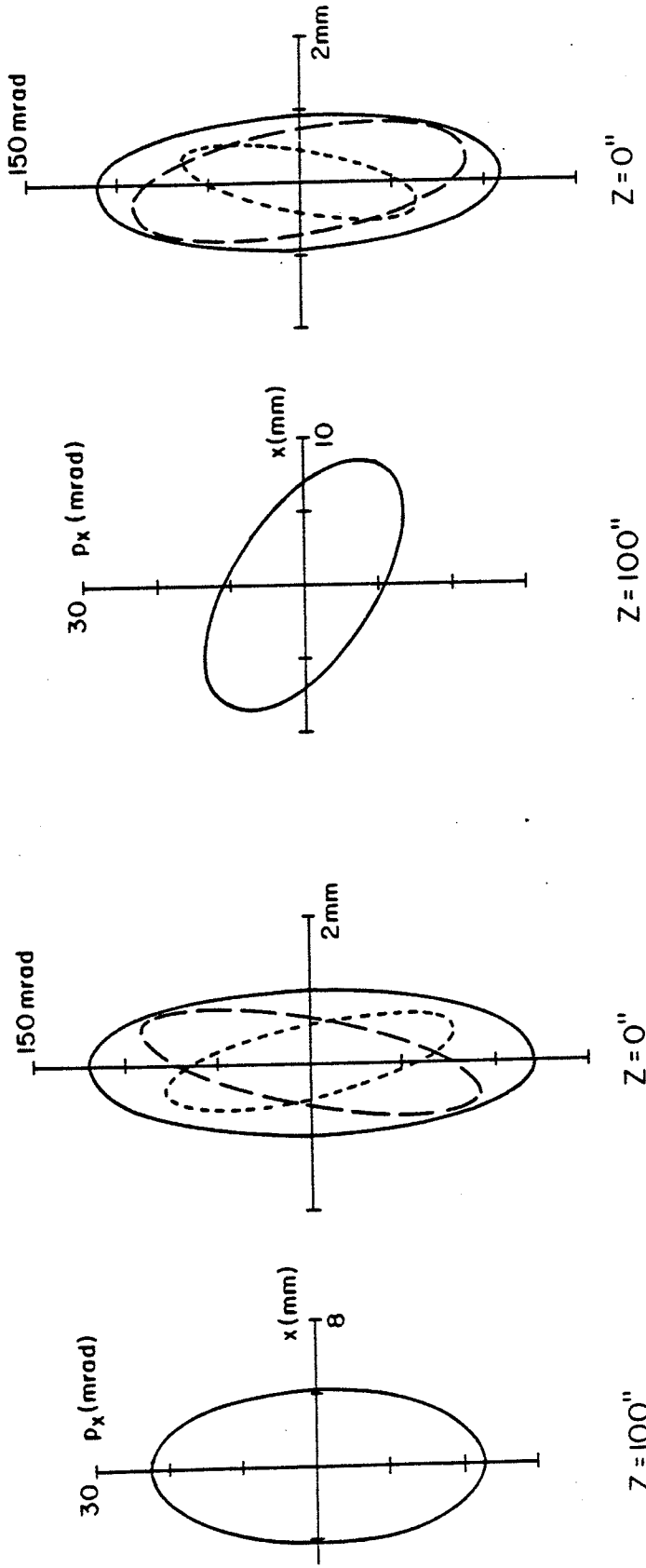
MSUX-80-313

Z = 0"

150 mrad

2mm

p_x (mrad)

30

x (mm)

10

Z = 100"

U^{46+} B_0 = 47.5 kgauss

V_{inj} = 20 kV

ϵ_i = 300 mm·mrad ϵ_f = 335 mm·mrad

Solenoid   60"-80"   B=1450 gauss

Z = 0"

150 mrad

2mm

V_{inj} = 10 kV

ϵ_i = 300 mm·mrad ϵ_f = 373 mm·mrad

Solenoid   60"-80"   B=-345 gauss

p_x (mrad)

30

x (mm)

8

Z = 100"

FIG. 27.   Same as Fig. 26, but for the U^{46+} ion.
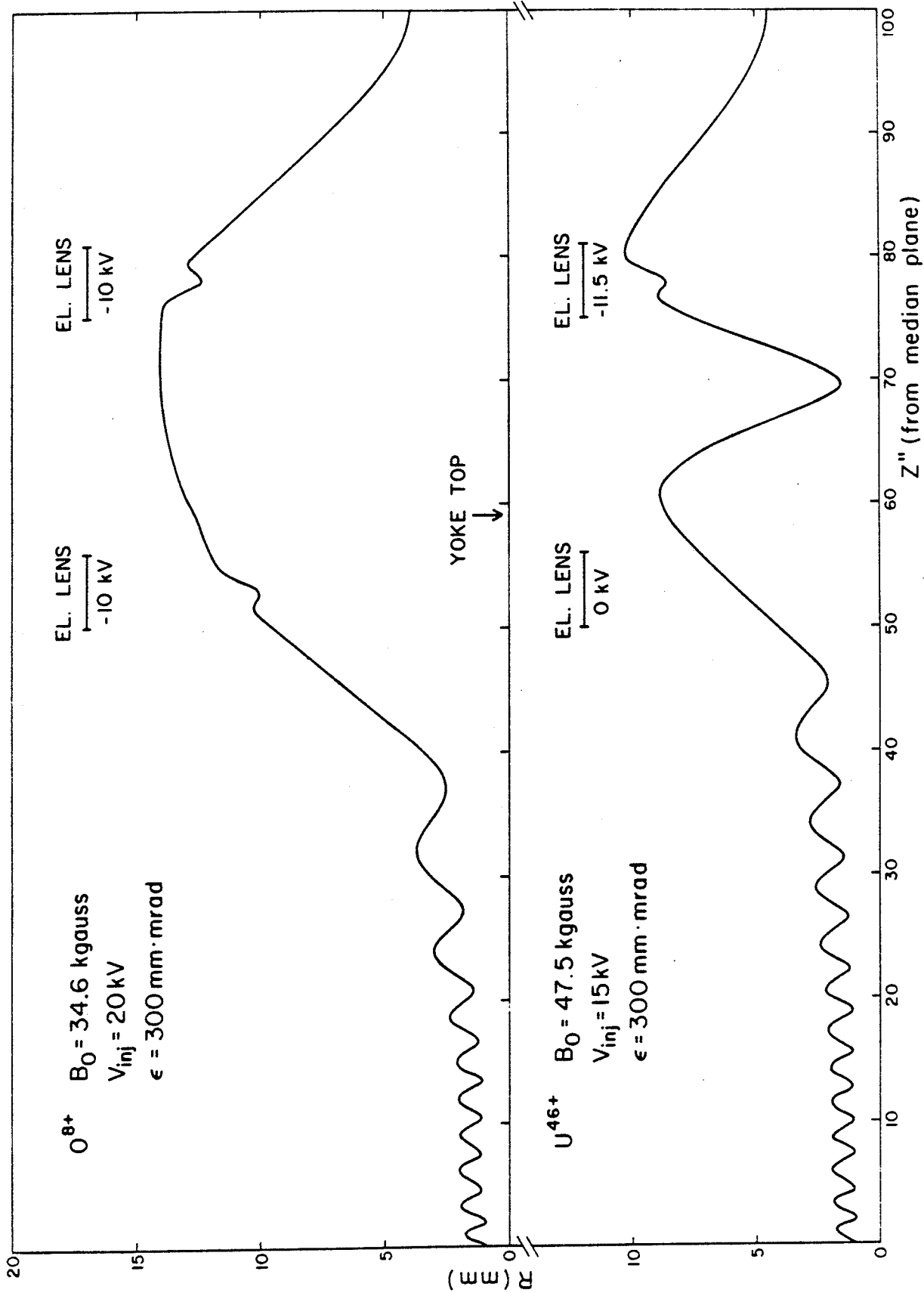
FIG. 28. Beam envelopes for the $q/A = 0.5$ and the U^{46+} ions using eingel lenses positioned as shown. Envelopes are traced backward from a 1 mm halfwidth waist at the median plane.

of 10 kV is sufficient to focus the beam, and a waist is preserved at the injection point. The corresponding phase spaces are shown in Fig. 29, and they can be directly compared with those of Fig. 25. The overall characteristics, including the emittance increase, are very similar to the solenoid case.

It can be noted, e.g. looking at the figures for the uranium ion, that the type of coupling obtained at the median plane between the (x, p_x) and (y, p_y) phase spaces is rather different, visually, in the case of the solenoid and of the einzel lens. However the net result in terms of the effective emittance, and its area, as seen at the cyclotron median plane is strictly the same. This result will be fully justified in the next section.

In summary a system of two einzel lenses also provides a suitable confinement method. In principle then the choice between the two can be left entirely to construction or cost considerations. However, as will be seen in the next section, the solenoid looks simpler and more effective when phase space matching is fully taken into account.

5.   Phase space matching

5.1   Theoretical analysis

We shall consider in this section the general problem of matching the injected beam emittance to the cyclotron acceptance. The former, here and in the following, is intended as the emittance at the injection point, where the magnetic
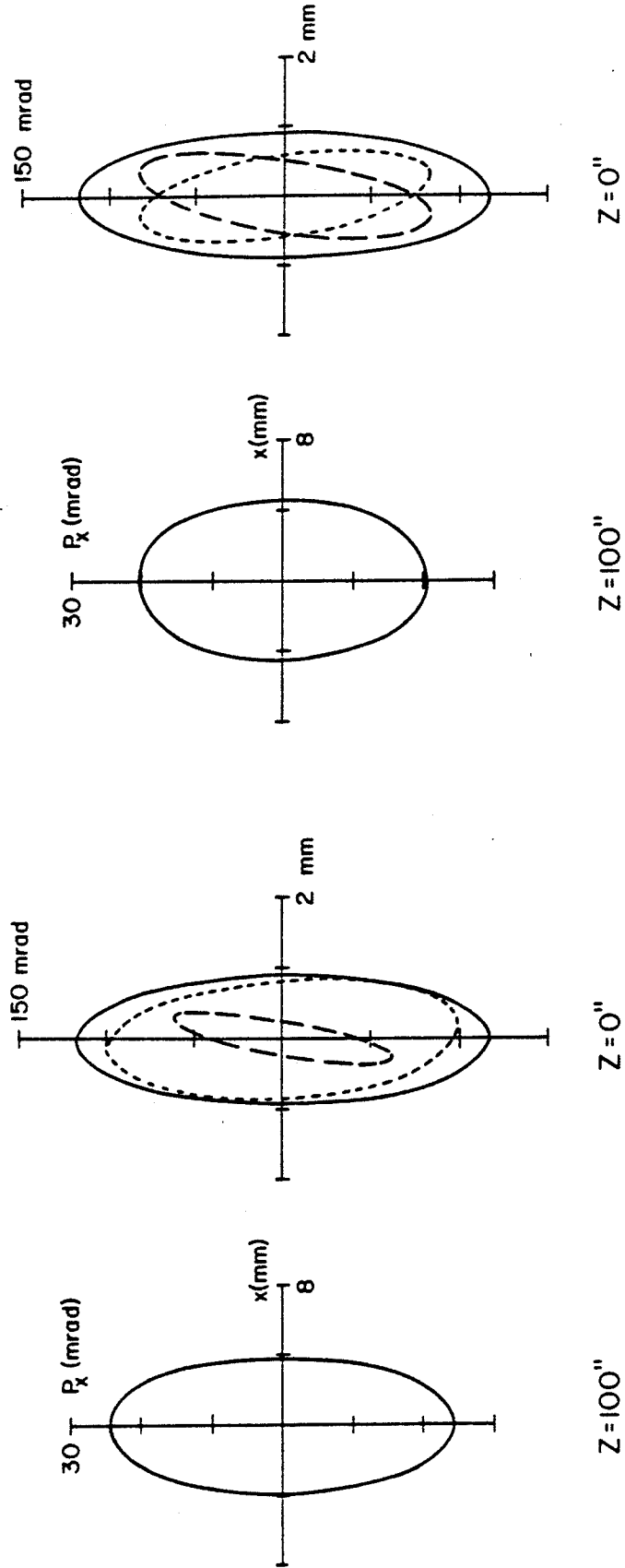
FIG. 29. Phase space behaviour for the two ions of Fig. 28, at the median plane and at the injection point.

field is zero, namely, in our case, z = 100". The cyclotron acceptance is defined at the inflector exit, i.e. at that position on the cyclotron median plane where the acceleration process begins. As we shall see in the following, and physically intuitive, both the yoke traversal and the inflection process must be considered in order to have a meaningful analysis. In other words, the inflection is far from negligible in determining the phase space behavior and in fact it plays an almost dominant role,.

In principle one would like to have:

- uncoupled (x, p_x), (y, p_y) phase spaces at the injection point (z = 100"). The ion source or a normal beam transport line will in effect usually produce such uncoupled phase spaces.
- uncoupled (x, p_x), (y, p_y) phase spaces at the inflector exit, matched to the cyclotron eigenellipse at that point.
- no beam emittance increase, in either subspace, between the injection point and the mirror exit.
- a well confined beam along the injection path.

We have already seen in Sec. 4 how the last requirement can be fulfilled. As for the first three, we recall that the longitudinal B_z field component couples very strongly the two transverse subspaces, via the particle rotation around the z-axis. This effect does not, in general, forbid the possibility to achieve the desired matching to the cyclotron acceptance in terms of the posture of the phase space

figures (e.g. waist or else). However, it will usually bring about an increase in the effective beam emittance and should therefore be carefully analyzed.

Strictly speaking, the notion of "phase space area", is defined only for a canonical set of coordinates. As explained in App. B, the usual linear (x, p_x) and (y, p_y) coordinates coincide with the canonical coordinates (x, P_x) and (y, P_y) when there is no coupling between the two subspaces. In this particular case they coincide only when the longitudinal field component is zero, namely at the injection point $(z = 100")$ and at the inflector exit. Of course we can always define, even in linear coordinates, an invariant four-dimension phase space volume (x, p_x, y, p_y), but this is seldom of any value.

The phase space behavior of the beam can therefore be best studied using canonical coordinates and considering at first separately the two main parts of the beam path, namely:

A.   motion in the hole up to the inflector entrance

B.   passage through the inflector

A.   <u>Motion in the hole up to the inflector entrance</u>

The coupling between the transverse subspaces persists even if the canonical coordinates (x, P_x) and (y, P_y) are used. However the coupling can be eliminated by using a

rotating Larmor frame (ξ, P_ξ), (η, P_η). That is to say, if
the canonical set of coordinates is rotated, at any given
distance along the z-axis, by an angle $\mu(z)$ expressed by:

$$\mu(z) = -\frac{1}{2} \int_{z_0}^{z} \frac{q\, B_z(z)}{P_z}\, dz \qquad (4)$$

This angle of rotation is determined only by the integral
of the longitudinal B_z field component, since we can trans-
form eq. (4) in:

$$\mu(z) = -\frac{1}{2\rho} \int_{z_0}^{z} \frac{B_z(z)}{B_0}\, dz \qquad (5)$$

where ρ is the radius of curvature of the ion and B_0 is
the field value at z = 0". In other words, using eq. (5)
we can determine the necessary rotation angle at any "z"
and in particular at the mirror entry, in order to have
a decoupled beam in the proper Larmor frame. A few comments
are in order:

i. The angle of rotation μ is obviously taken as 0° at
    the z = 100" point.

ii. As a consequence of eq. (5) the transfer of a beam
    from a point with $B_z = 0$ to a point with $B_z \neq 0$ can
    be made without increase in the canonical subspace
    areas (x, P_x) and (y, P_y), only if a rotating frame with
    μ as given by eq. (5) is used. However, there will
    always be a nonconservation of the areas in the linear
    subspaces (x, p_x) and (y, p_y), which is physically due
    to the mentioned coupling between the two transversal
    subspaces.

iii. A control of the rotation angle μ can be accomplished
by any device, like a solenoid, which produces a longi-
tudinal field component. This will be discussed later
in a quantitative way.

A particularly simple case, which illustrates well
the kind of linear phase space area increase to be expected,
is when a symmetric beam (in the two transversal subspaces)
is injected at z = 100", and a symmetric beam is obtained
at z = 0". As we have seen in Sec. 4, this can be achieved
by either a solenoid or a system of einzel lenses. In this
case the angle of rotation μ, because of the symmetry of
the beam, plays no role and the emittance transformation
in the usual linear coordinates can be easily calculated
using eq. B-16 of App. B. The result is:

$$\varepsilon = \sqrt{\varepsilon_{inj}^2 + \pi^2 \frac{r_b^4}{4 \rho^2}} \qquad (6)$$

where ε_{inj} is the injected phase space area of the uncoupled
and symmetric beam at z = 100" with divergence expressed
in radians, r_b is the beam size (halfwidth) at the median
plane and ρ is the ion radius of curvature in the B_o field.
This effect, which does not depend at all on the details
of the magnetic field along the injection path, fully justifies
the results obtained in Sec. 4, which dealt, as will be
recalled, with symmetric beams in the two transverse subspaces.

Coming back to the general question of phase space
increase, one might argue that the ultimate result of the

entire injection is to let the beam go between two points, i.e. z = 100" and the median plane via a 90° deflection, where the longitudinal component of the fields is zero. That is to say that in these two points linear and canonical phase space areas coincide. One could think, then, that it may be possible to inject and deflect the beam into the median plane in such a way as to eliminate the coupling between the two transversal subspaces and, ultimately, the variation of the phase space areas.

It is therefore necessary to carry out a careful analysis of the behavior of phase space in the inflection process. As we shall see, this depends very much upon the kind of inflector chosen. The considerations which follow are made for a mirror.

B. Passage through the inflector

It turns out that it is relatively easy to express the transfer matrix of the mirror when linear coordinates are used. This is shown, and the matrix given, in App. A. As a consequence, an easy way to obtain the linear (x, P_x) (z, P_z) phase spaces at the mirror exit is by the following procedure:

- the beam at the mirror entrance is expressed in the Larmor frame coordinates $(\xi, P_\xi)(\eta, P_\eta)$, rotated by the angle μ in order to assure decoupling (See App. B).
- the canonical coordinates are transformed into linear coordinates. (matrix T)

-     the latter coordinates are rotated by an angle $-\mu$. (matrix R)

-     the mirror transfer matrix M (in linear coordinates) is applied.

Symbolically we can write:

$$\begin{vmatrix} x \\ p_x \\ z \\ p_z \end{vmatrix} = M \cdot R \cdot T \begin{vmatrix} \xi \\ p_\xi \\ \eta \\ p_\eta \end{vmatrix}$$

The total transfer matrix thus obtained has obviously Det = 1, to obey Liouville's theorem. Also, in order to give at the mirror exit a decoupled beam, and therefore a zero increase in the subspaces areas, the matrix should be of the form:

$$\begin{vmatrix} a_{11} & a_{12} & 0 & 0 \\ a_{21} & a_{22} & 0 & 0 \\ 0 & 0 & a_{33} & a_{34} \\ 0 & 0 & a_{43} & a_{44} \end{vmatrix}$$

It turns out that in the case of a mirror this is impossible whatever angle μ is chosen. In this respect let us just recall that μ is in principle variable at will if a solenoid is used along the injection line.

As a consequence an increase in the phase space area, due to coupling, must be expected. In the following paragraph we shall present detailed numerical calculations concerning this effect.

5.2 Phase space increase: numerical results

In order to give results of general validity we have made the following assumptions:

- injection, at z = 100", of an uncoupled beam in the two transverse subspaces.

- requirement, at the mirror exit, of waists in both linear phase spaces. Their size should not necessarily be equal in the (x,p_x), (z,p_z) planes.

- accordingly we have selected a beam size at the waists varying between 2 and 5 mm in either the x or z dimension, with a beam emittance at the mirror exit of 500 mm mrad.

- rotation angle μ as given by the existing cyclotron field, plus the field produced by the solenoid as needed for beam confinement purposes (see Sec. 4).

Strictly speaking, the problem has six unknowns, which define the uncoupled beam in the (x,p_x) and (y,p_y) planes at z = 100", and six parameters which define the two waists at the mirror exit. Knowing the total transfer matrix between z = 100" and the mirror exit we can therefore solve the corresponding linear system. The solution does not always exist, since constraints have to be made in order to define a real beam. However, if the solution exists, we can calculate the phase space area increase produced at the mirror exit.

The beam for which calculations have been carried out is a fully stripped light ion beam with q/A = 0.5, an injection

voltage V = 20 KV, and a central field B_o = 34.6 Kgauss. The beam confinement is obtained with the solenoid between z = 60" and z = 80" already described in Sec. 4 which produces a field of 660 Gauss. The corresponding rotation angle for such a beam is μ = 31.3°.

The phase space area increase is better appreciated if the beam emittance which must be injected at z = 100" is presented for a fixed emittance of 500 mm mrad in both transverse phase spaces at the mirror exit. This is shown in Fig. 30, where the latter values are written at a number of points in the X_w, Z_w plane, where X_w and Z_w are the waists halfwidth at the mirror exit. It should be remarked that at z = 100" the phase space areas are always equal in the (x, p_x), (y, p_y) planes. The phase spaces to be injected are not generally waists nor are they symmetric, although they are always rigorously decoupled. As an example, the linear phase spaces for the particular case of $X_w = Z_w$ = 1.5 mm are presented in Fig. 31 in three positions, namely at z = 100", mirror entrance and mirror exit. The coupling at the mirror exit is quite evident and is responsible for the observed phase space area increase, from 300 to 500 mm mrad. All data of Fig. 30 should therefore be interpreted in the sense explained by Fig. 31. From Fig. 30 it is apparent that the solution does not always exist, and that when it exists, phase space area increase of at least 50% and up to a factor 3 can be expected, or in other terms, a corresponding decrease in beam luminosity.
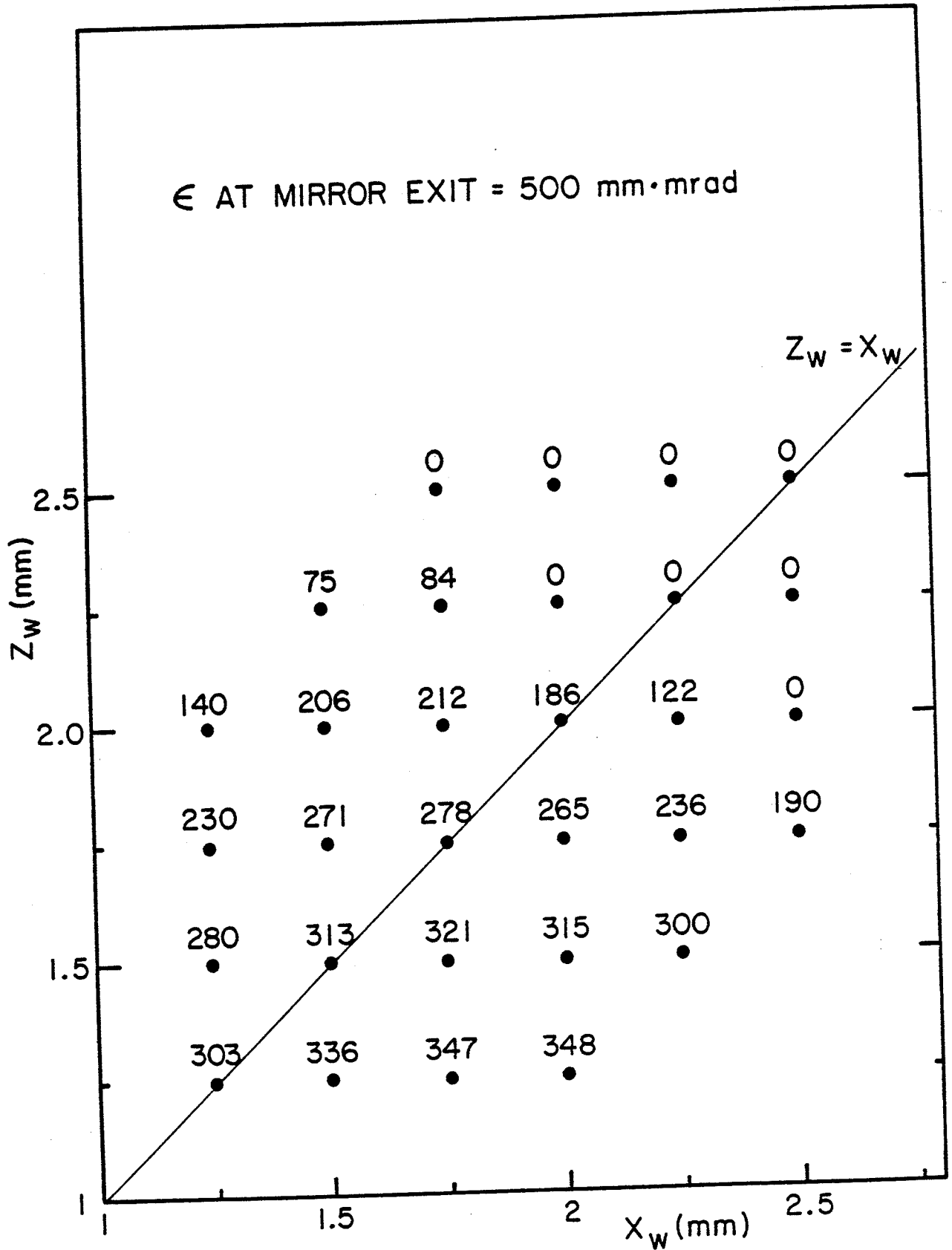
FIG. 30. Beam emittances at z = 100 inches, which produce waists with a 500 mm.mrad emittance at the mirror exit, in either the (x, p_x) or (z, p_z) phase spaces. The x_w and z_w coordinates represent the waist halfwidths at this latter point. For points labelled 0 no solution exists.
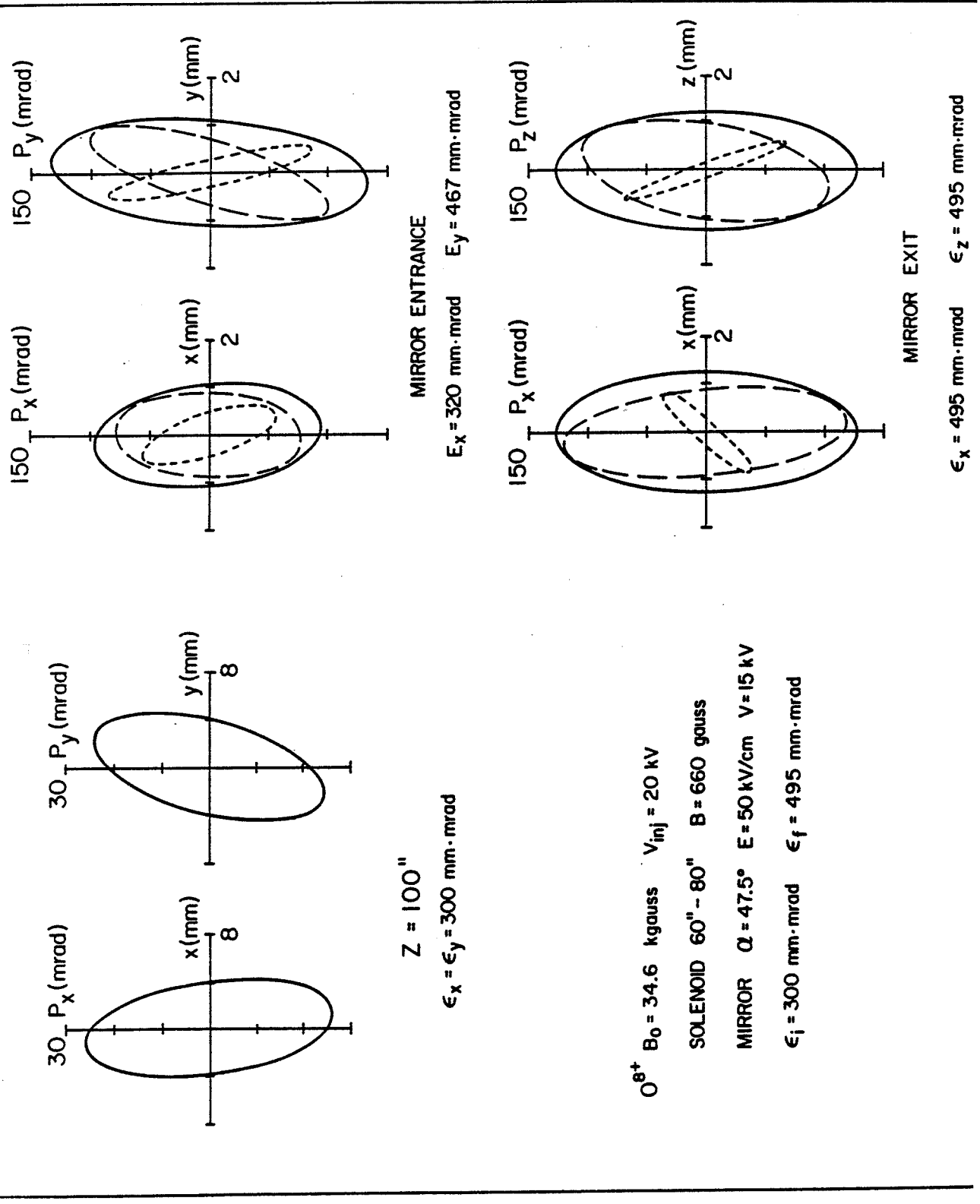
FIG. 31. Phase space behaviour of the q/A = 0.5 ion at z = 100 inches, mirror entrance, and mirror exit. Dashed lines indicate the area pertaining to the particular phase space, and dotted lines the area arising from the coupling with the other phase space. Coupling between the two subspaces produces the total area shown by a solid line.

A further optimization is possible by considering that
the injected phase space area, for a given phase space ellipse
at the mirror exit, is a function of the rotation angle
μ. The injected phase space is a periodic function of μ,
with periodicity of 180° for the phase space figure and
90° for the area. This latter case corresponds to an exchange
of phase space figure between the (x, p_x) and the (y, p_y)
planes.

For the same matching conditions of Fig. 31 ($X_w = Z_w = 1.5$ mm,
$\varepsilon = 500$ mm mrad), the injected phase space area is presented
in Fig. 32 as a function of the rotation angle μ. Note
again that the solution exists only for particular values
of μ, i.e. in the range of 5° to 50°. The maximum of the
injected phase space area is 330 mm mrad for $\mu = 40^{\circ}$ and
is rather stable for small variations of the angle μ.

From these results it follows that a control of the
rotation angle μ is quite important in order to obtain an
optimized matching. To assure a variation of μ of 90°
we need, in our case, an integral of the B_z field of about
90 kgauss cm, which, for a 20" long solenoid, corresponds
to a field of about 2 Kgauss. If we assume the μ variation
to be in the range of $\pm 45^{\circ}$, therefore adding or subtracting
the solenoid field from the given yoke field, a field of
1 kgauss will suffice.

According to these considerations we have carried out
an optimization of the angle μ so as to obtain a maximum
of the injected phase space area for all cases presented

ε at mirror exit = 500 mm·mrad

Double waist with $X_w = Z_w = 1.5$ mm

$$\frac{T_{in}}{A} = 10 \text{ keV/n}$$

$Z/A = .5$ $B_0 = 34.6$ kgauss
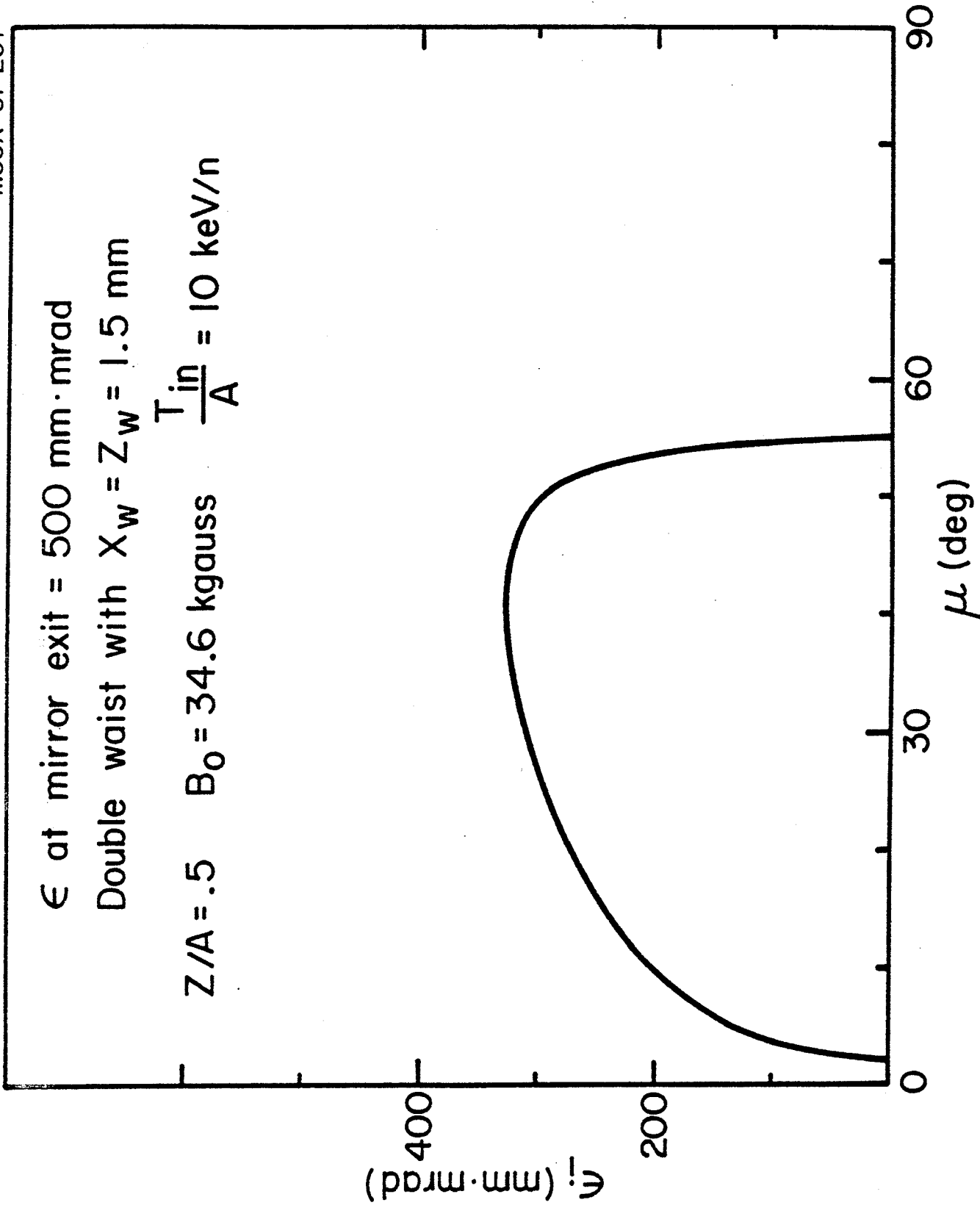
FIG. 32. Variation of the emittance of the beam to be injected at
$z = 100$ inches, as a function of the angle μ, in order to obtain a
500 mm·mrad emittance at the mirror exit.

in Fig. 30. The results are shown in Fig. 33 and they point out that very dramatic improvements can be obtained this way. However, sizable increases of the phase space area between the injection point and the mirror exit are still present and, as proved by the preceding arguments, cannot be eliminated unless a different inflector is chosen. For most cases of practical importance shown in Fig. 33, the increase is however tolerable, given the cyclotron acceptance.

The hyperboloid inflector[11] is, to the best of our knowledge, the only known device which can produce a decoupled beam, in linear coordinates, in the cyclotron with no phase space area increase, provided that the rotation angle is properly adjusted. This type of inflector requires however a rather large space in the median plane, space which looks right now incompatible with the design of a central region for a superconducting cyclotron.

$\in$ AT MIRROR EXIT = 500 mm·mrad

LEGEND

INJECTED AREA (mm·mrad) AT Z = 100"

$[\mu]$ ROTATION ANGLE (deg)
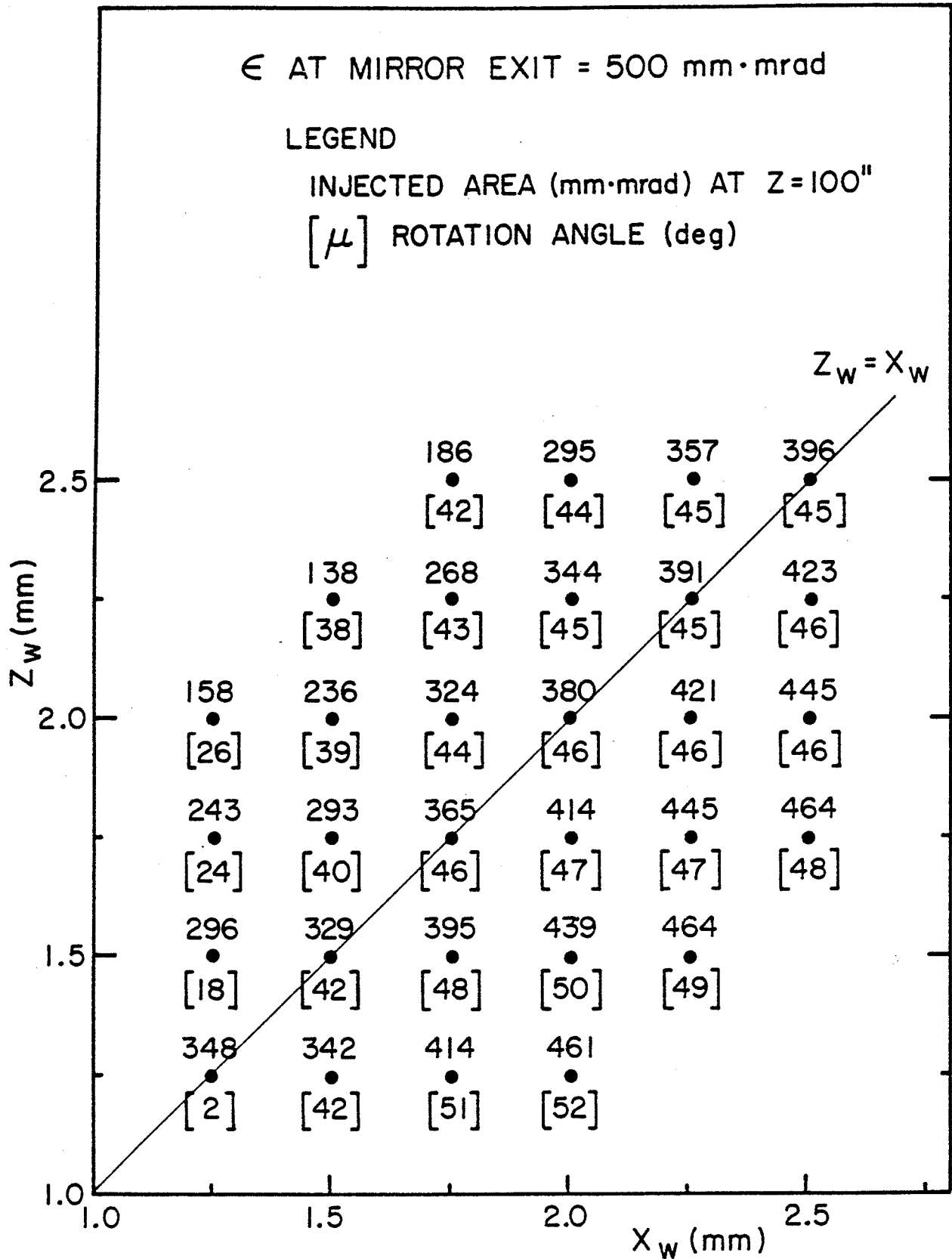

FIG. 33. Beam emittances at z = 100 inches which produce waists with a 500 mm.mrad emittance in either the (x, p_x) or (z, p_z) phase spaces at the mirror exit. The optimized value of the rotation angle μ is in brackets (see text for details). The x_w and z_w coordinates represent the waist halfwidths at the mirror exit.

Conclusions

This study shows that axial injection in superconducting cyclotrons is indeed feasible, with injection voltages rather similar to those encountered in conventional cyclotrons.

An electrostatic mirror seems adequate, although different inflectors could obviously be used. Space requirements do however pose very definite limitations. Injection off the magnet axis may be necessary, even though a much more detailed study of the center region geometry will be needed if an actual system is to be built.

The injection scheme presented here, with two deflectors for steering the beam off the axis, and a solenoid (or two einzel lenses) for matching and confinement purposes, seems a viable option and certainly one of the simplest. Obviously, one may want to properly investigate some more cases of beam matching. We believe however that the general conclusions stated here with respect to the emittance increase will remain valid.

We list here a few comments concerning the building of an actual system:

- in a superconducting cyclotron it will be advantageous to have the injection path from the bottom, and the mirror or whatever inflector, inserted from the top. This choice minimizes problems associated with lifting the upper half of the magnet, an important operation in these machines in order to have access to the median plane.

- The ion source will probably be far away from the cyclotron because of physical size, stray magnetic fields, easy access, etc.

- A suitable transport line, must then be provided which guarantees the matching at the injection point, performs charge state analysis of the ions, etc. If this line is too long there could be problems associated with pickup and stripping by heavy ions in the residual vacuum. At the low energies envisaged in this study, this could conceivably pose vacuum requirements of the order of 10^{-8} torr. One possible way out could be to accelerate the beam at fairly higher energy up to close to the injection point, and then decelerate it for the final injection.

- The relative emptiness of the injection path through the yoke leaves ample space for the buncher and diagnostic elements of all kinds. An interesting aspect is how to make sure, in actual operation, that the beam is properly aligned off the axis at the mirror. Since as shown before, this is a four parameter problem, a very accurate computed guideline, based on precise field measurements, both magnetic and electric, is necessary. Tests will have to be done, before inserting the mirror, with special diagnostic equipment in the median plane. The high reproducibility of the magnetic field in superconducting cyclotrons, due to the iron saturation, will assure, after these measurements, that the proper injection conditions are met.

Therefore, even though a few details should still
be worked out for building an actual system, we would like
to conclude that superconducting cyclotrons seem capable
of taking full advantage of the new ion sources being now
developed.

Table I

0^{8+}	$B_O = 34.6$ Kgauss	U^{46+}	$B_O = 47.5$ Kgauss
V_{inj} (kV)	ρ (cm)	V_{inj} (kV)	ρ (cm)
10	.5855	5	.4875
15	.7207	10	.6894
20	.8322	15	.8444
25	.9304	20	.9750
30	1.0192	25	1.0901
35	1.1009		

Appendix A

The inflector

Calculations of the properties of a mirror for an axial
injection system have been published by Hazewindus.[16]
Since some approximations intorduced in the equations of
motion led to errors in the predicted phase space behaviour
a complete analysis is reported here using essentially the
same notation.

A schematic view of the inflector is presented in fig. Al.
The inflector is defined by two parallel planes which make
an angle α with the median plane defined by z=0. The upper
plane is actually a grid of wires at zero potential to make
the inflector as transparent as possible to the beam. The
other electrode is connected to a positive voltage; the
electric field presents only two components, E_y and E_z which
bend the incoming positively charged beam into the median
plane.

The equations of motion

In a magnetic and electric field the equation of motion
is, with time t as independent variable

$$m \frac{d\vec{v}}{dt} = q(\vec{E} + \vec{v} \times \vec{B})$$
(A1)

The components of a uniform magnetic field $B=B_o$ pointing
in the negative z direction, so that after inflection the
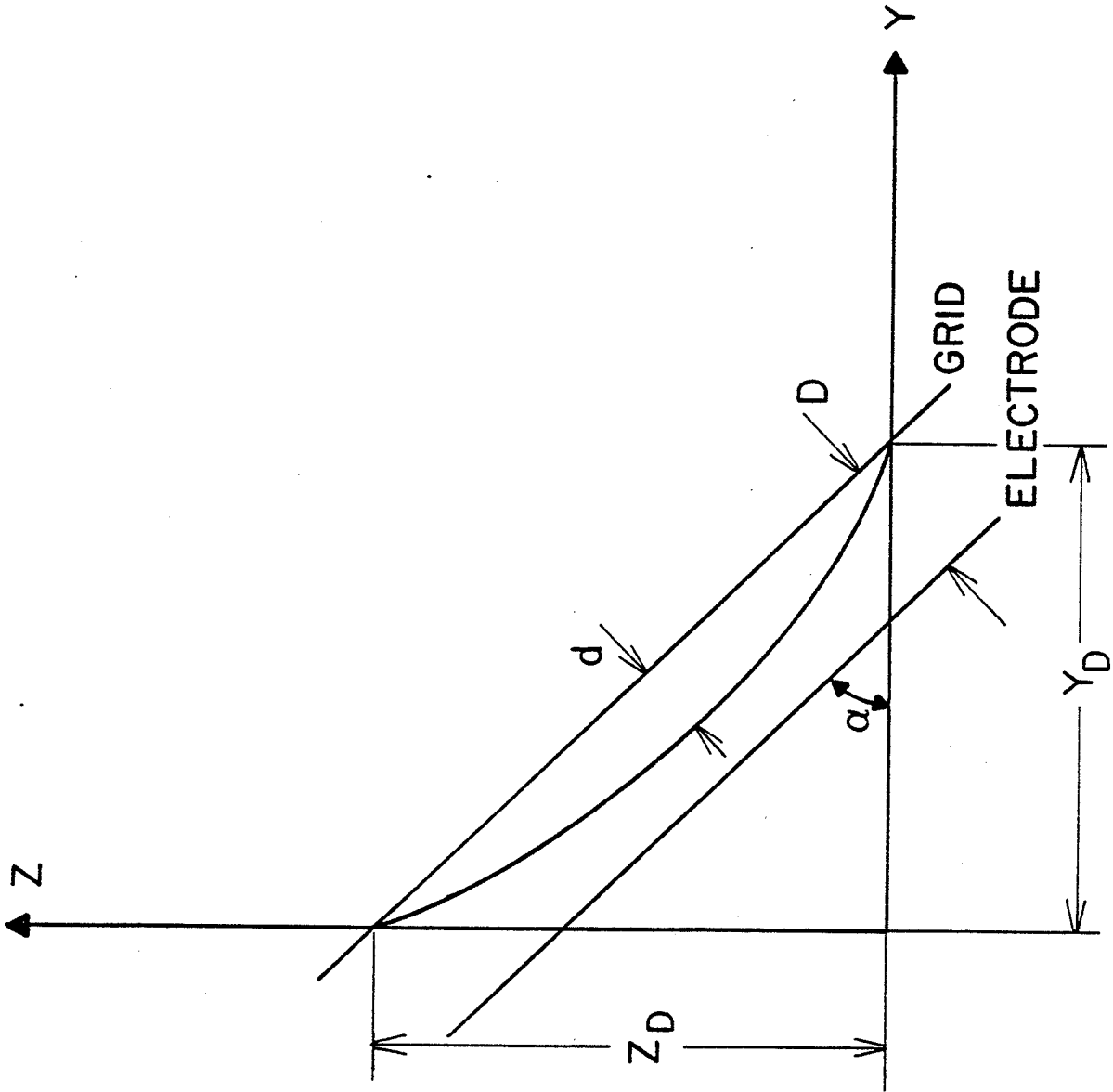positive ion rotates anticlockwise, are given by:

FIG. A1. Schematic view of the inflector.

$$B_z = -B_o \qquad B_x = B_y = 0$$

The electric field components can be derived from the inflector geometry as

$$E_x = 0 \qquad E_y = E\sin\alpha \qquad E_z = E\cos\alpha$$

where E is the total electric field and α is the angle between the inflector plane and the z=0 plane.

The magnetic field B_o defines for a beam of ions with charge state q, rest mass m_o and momentum p_o, the angular velocity

$$\omega = \frac{qB_o}{m_o}$$

and the radius of curvature

$$\rho = \frac{p_o}{qB_o} = \left(\frac{2V_o}{\omega B_o}\right)^{\frac{1}{2}}$$

where V_o is the source voltage. Introducing τ as dimensionless independent variable, defined by:

$$\tau = \omega t$$

and new dimensionless coordinates

$$X = \frac{x}{\rho} \qquad Y = \frac{y}{\rho} \qquad Z = \frac{z}{\rho}$$

so that

$$\dot{X} = \frac{p_x}{p_o} \qquad \dot{Y} = \frac{p_y}{p_o} \qquad \dot{Z} = \frac{p_z}{p_o}$$

37

the equations of motion become:

$$\ddot{X} = -\dot{Y}$$

$$\ddot{Y} = \frac{E}{\omega B \rho} \sin\alpha + \dot{X} \qquad (A2)$$

$$\ddot{Z} = \frac{E}{\omega B \rho} \cos\alpha$$

The general solution can be written as:

$$X = (X_0 - \dot{Y}_0) + \dot{Y}_0 \cos\tau + (\dot{X}_0 + \frac{E}{\omega B \rho} \sin\alpha) \sin\tau - \frac{E}{\omega B \rho} \sin\alpha \cdot \tau$$

$$Y = (Y_0 + \dot{X}_0 + \frac{E}{\omega B \rho} \sin\alpha) - (\dot{X}_0 + \frac{E}{\omega B \rho} \sin\alpha)\cos\tau + \dot{Y}_0 \sin\tau \quad (A3)$$

$$Z = Z_0 + \dot{Z}_0 \tau + \frac{1}{2} \frac{E}{\omega B \rho} \cos\alpha \, \tau^2$$

The inflection in the median plane

The central ray of the incoming beam at the entrance
of the inflector has the following coordinates and momenta:

$$X_0 = Y_0 = 0 \qquad Z_0 = Z_D$$

$$\dot{X}_0 = \dot{Y}_0 = 0 \qquad \dot{Z}_0 = \frac{p_z}{p_0} = -1$$

The inflection in the median plane is equivalent to the
condition

$$Z = 0 \qquad \dot{Z} = 0$$

at the exit of the inflector. These constraints applied
to the general solution (A3) define the system

$$\frac{E}{\omega B \rho} \cos\alpha \, \tau = 1 \qquad\qquad \text{constraint } \dot{Z} = 0$$

$$Z_D = \tau - \frac{1}{2} \frac{E}{\omega B \rho} \cos\alpha \, \tau^2 \qquad\qquad " \qquad Z = 0 \qquad (A4)$$

$$Z_D = Y \, \text{tg} \, \alpha = \frac{E}{\omega B \rho} \sin\alpha (1 - \cos\tau) \, \text{tg}\alpha \qquad " \qquad Z = 0 \text{ at the}$$

$$\text{inflector exit}$$

The system can be easily reduced to (τ_D = transit time in the inflector)

$$\frac{1}{2} \tau_D^2 = tg^2\alpha \, (1-\cos\tau_D)$$

and

$$z_D = \frac{1}{2} \tau_D \; , \qquad E = \frac{\omega B\rho}{\tau_D} \frac{1}{\cos\alpha}$$

(A5)

Some general conclusions can be drawn from equations A5.

- The inflector angle α and the curvature radius ρ of the beam define the geometry of the inflector. A fixed geometry implies a fixed ρ, that is a "constant orbit" mode of operation of the cyclotron. The inflector angle α must be $\geq 45°$. Strictly speaking, $\alpha = 45°$ is possible only in the absence of the magnetic field B_o.

- The electric field is the main parameter limiting the inflector performance. Note that for fixed E any increase in ρ implies an increase in the dimensions of the inflector.

Using the relations A5 the general solution (eq. A3) becomes now

$$X = -\frac{tg\alpha}{\tau_D} (\tau-\sin\tau) + X_o + (\sin\tau)\dot{X}_o - (1-\cos\tau) \, \dot{Y}_o$$

$$Y = \frac{tg\alpha}{\tau_D} (1-\cos\tau) + (1-\cos\tau) \, \dot{X}_o + Y_o + (\sin\tau) \, \dot{Y}_o \qquad \text{(A6)}$$

$$Z = (Z_o-Z_D) + \frac{1}{2} \tau_D + \dot{Z}_o\tau + \frac{1}{2} \frac{\tau^2}{\tau_D}$$

39

At the exit of the inflector the central ray of the beam will have the following set of coordinates and momenta (all expressed in dimensionless units)

$$Z = 0 \qquad\qquad \dot{Z} = 0$$

$$X_D = -tg\alpha \; \frac{\tau_D - \sin\tau_D}{\tau_D} \qquad\qquad \dot{X}_D = -tg\alpha \; \frac{1 - \cos\tau_D}{\tau_D}$$

$$Y_D = tg\alpha \; \frac{1 - \cos\tau_D}{\tau_D} \qquad\qquad \dot{Y}_D = tg\alpha \; \frac{\sin\tau_D}{\tau_D}$$

Other important parameters at the exit of the inflector are: (See fig. A2)

$$R_D = \frac{1}{\tau_D} \; tg\alpha \; \left[(\tau_D - \sin\tau_D)^2 + (1 - \cos\tau_D)^2 \right]^{\frac{1}{2}}$$

$$tg\theta = \frac{\tau_D - \sin\tau_D}{1 - \cos\tau_D}$$

$$\phi = \frac{\tau_D}{2}$$

$$tg\gamma = \frac{2(1 - \cos\tau_D) - \tau_D \sin\tau_D}{\tau_D (1 - \cos\tau_D)}$$

Maximum displacement inside the inflector

The maximum displacement of the central ray, inside the inflector, from the grid corresponds to

$$\frac{dZ}{dY} = -tg\alpha$$

that is

$$\dot{Z}/\dot{Y} = -tg\alpha$$

40
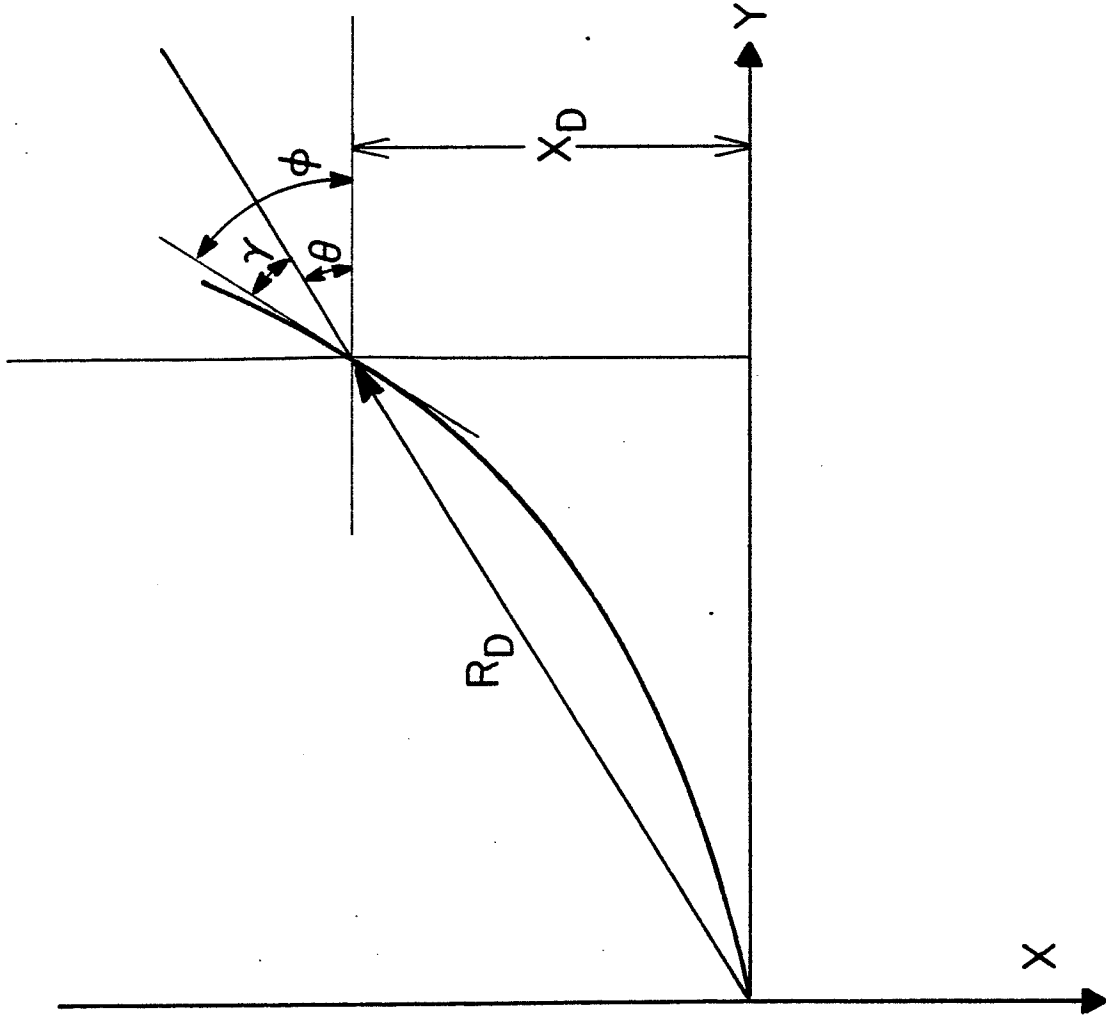
FIG. A2. Definition of the parameters used at the inflector exit.

which after substitution gives the relation

$$\tau_M + tg^2\alpha \ \sin\tau_M = \tau_D$$

The value of the maximum displacement d is (dimensionless unit)

$$d = \frac{1}{2\tau_D} \left[-\tau_M^2 + 2\tau_D\tau_M - 2tg^2\alpha(1-\cos\tau_M) \right] \cos\alpha$$

For an ion with a given starting condition at the plane $z = z_D$ the corresponding time is given, to first order, by

$$\tau_e = \tau_M + \frac{-\sin\tau_M tg\alpha \dot{X}_0 - \cos\tau_M tg\alpha \dot{Y}_0 + \frac{\Delta p}{p}}{\frac{1 + tg^2\alpha\cos\tau_M}{\tau_D}}$$

and the corresponding displacement is

$$d_e = d + \left[-tg\alpha(1-\cos\tau_M)\dot{X}_0 - tg\alpha\sin\tau_M\dot{Y}_0 + \tau_M\frac{\Delta p}{p} \right]\cos\alpha \ .$$

To assure that the beam does not hit the electrode we assume $D \approx 2d$ where D is the distance between electrodes, determining together with the electric field E the inflector voltage.

Choice of the inflector parameters

The study of the region sets the energy of fully stripped ions for good centering after a few turns at a value of 10 keV/n.

For the K800 the magnetic field corresponding to the maximum energy for fully stripped ions is 34.6 kgauss. We obtain

$$q/A = 0.5 \quad B_o = 34.6 \quad V_o = 20 \text{ kV} \quad \rho = 8.32214 \text{ mm}$$

Introducing an upper limit of 50 kV/cm for the electric field in the inflector we obtain

$$E = \frac{2V_o}{\rho \tau_D \cos\alpha} \leq 50 \text{ kV/cm}$$

$$\tau_D \cos\alpha \geq 0.96129$$

This relation is verified for

$$\alpha = 47.5^\circ$$

and it follows that:

$$\tau_D = 1.43544 \quad \tau_M = 0.68341 \quad d = 1.8801 \text{ mm}$$

$$Z_D = 5.973 \text{ mm} \qquad R_D = 6.154 \text{ mm}$$
$$Y_D = 5.473 \text{ mm} \qquad \phi = 41.122^\circ$$
$$X_D = 2.813 \text{ mm} \qquad \gamma = 13.922^\circ$$

$$E = 49.56 \text{ kV/cm} \quad D = 3.75 \text{ mm} \quad V_D = 18.58 \text{ kV}$$

Scaling laws

The scaling law for all other ions is defined by the condition

$$\rho = \text{const}$$

We obtain for the main parameters; injection voltage V_o, electric field in the deflector E, inflector voltage V_D,

- redefinition of a new set of coordinates in the plane $z = 0$ corresponding to the Y_c axis pointing along the direction of motion of the central particle (subscript co)

- calculations of the coordinates and momenta in the plane $Y_c = 0$ (subscript c) therefore defining a "virtual" source of phase space for the cyclotron.

All the calculations will be carried out to first order in X_o, $\dot{X}_o$, Y_o, $\dot{Y}_o$, $\frac{\Delta p}{p}$ (all dimensionless) using the eq. (A6). When considering the motion in the magnetic field only terms containing $tg\alpha$ or τ_D will be dropped, since these terms come from the electric field of the mirror.

The momentum spread $\frac{\Delta p}{p}$ is introduced in the equation through the z component of the momentum at the plane $z = z_D$. Defining $p = p_o(1 + \frac{\Delta p}{p_o})$ to first order is

$$\dot{z}_o = \frac{p_z}{p_o} = -(1 + \frac{\Delta p}{p_o})$$

For each of the parts specified at the beginning of this section the transit time variation $\Delta\tau$ with respect to the central ray transit time τ will be calculated and then substituted in eq (A6) to obtain the final values of coordinates and momenta.

Since we are looking for first order variations we have to consider only the first order dependence on $\Delta\tau$ and the first order dependence of $\Delta\tau$ on the starting condition.

We can subsequently expand eq (A6) to first order in $\Delta\tau$ obtaining (τ is the transit time for the centray ray)

$$V_o \propto \omega \, B_o$$

$$E \propto \omega \, B_o \, .$$

$$V_D \propto \omega \, B_o$$

The product ωB is maximum on the focusing limit of the cyclo-
tron. If the maximum injection voltage along the focusing
line is of the order of 20 kV the minimum for the K800 will
be V_o = 4.1 kV (for the particle with q/A = 0.1 B_o = 35 kgauss).

Effect of the mirror on phase space

The motion of a bunch of ions through the mirror will
be considered with respect to the coordinates indicated
in the figures A1 and A2. The ions start at the plane
$Z = Z_D$ which corresponds to the entrance to the mirror for
the central ray.

The advantage of this choice is the use of the standard
notation for the phase space (defined in a plane perpendicular
to the longitudinal motion). A "virtual" phase space is
therefore defined at the plane $Z = Z_D$, in the sense that
the phase space at this position is the one obtained when
the mirror is not inserted.

The calculations for the passage of the ions through
the mirror are divided in the following parts:

-   motion from the plane $Z = Z_D$ to the mirror entrance
    (subscript 1)
-   motion through the mirror up to the mirror exit (sub-
    script 2)

43

$$X_1 = X_o \qquad\qquad \dot{X}_1 = \dot{X}_o$$

$$Y_1 = Y_o \qquad\qquad \dot{Y}_1 = \dot{Y}_o$$

$$Z_1 = Z_D - tg\alpha Y_o \qquad \dot{Z}_1 = \dot{Z}_o = -(1 + \frac{\Delta p}{p})$$

ii) Motion inside the mirror

Substituting the equation of motion (A7) in the equation of the grid and recalling that for the central ray the transit time is τ_D, the transit time variation is given by

$$\tau_{21} - \tau_D = -(2\sin\frac{\tau_D}{2} \, tg \, \frac{\tau_D}{2})\dot{X}_o - (2\sin\frac{\tau_D}{2})\dot{Y}_o + (2tg\frac{\tau_D}{2}) \frac{\Delta p}{p}$$

Therefore at the mirror exit:

$$X_2 = \frac{-tg\alpha}{\tau_D}(\tau_D - \sin\tau_D) + X_o + 2tg \, \tau_D/2 \, \dot{X}_o - \frac{1-\cos\tau_D}{\cos\tau_D/2} \, \frac{\Delta p}{p}$$

$$Y_2 = \frac{tg\alpha}{\tau_D}(1-\cos\tau_D) + Y_o + 2\sin\tau_D/2 \, \frac{\Delta p}{p}$$

$$Z_2 = -tg\alpha \, Y_o - \tau_D \, \frac{\Delta p}{p}$$

$$\dot{X}_2 = \frac{-tg\alpha}{\tau_D}(1-\cos\tau_D) + \dot{X}_o - 2\sin\tau_D/2 \, \frac{\Delta p}{p}$$

$$\dot{Y}_2 = \frac{tg\alpha}{\tau_D}\sin\tau_D + tg\tau_D/2 \, \dot{X}_o + \frac{\cos\tau_D}{\cos\tau_{D/2}} \, \frac{\Delta p}{p}$$

$$\dot{Z}_2 = \frac{-tg\alpha_{D/2}}{tg\alpha} \, \dot{X}_o - \frac{1}{tg\alpha} \, \dot{Y}_o - (1 - \frac{1}{tg\alpha\cos\tau_{D/2}}) \, \frac{\Delta p}{p}$$

iii) Rototranslation of the coordinates

We define a new coordinate system centered on the exit point of the mirror for the central ray and with the Y_c

$$X = -\frac{tg\alpha}{\tau_D}\left[\tau-\sin\tau+(1-\cos\tau)\Delta\tau\right] + X_0+(\sin\tau+\Delta\tau\cos\tau)\dot{X}_0-(1-\cos\tau+\Delta\tau\sin\tau)\dot{Y}_0$$

$$\dot{X} = -\frac{tg\alpha}{\tau_D}(1-\cos\tau+\Delta\tau\sin\tau) + (\cos\tau-\Delta\tau\sin\tau)\dot{X}_0-(\sin\tau+\Delta\tau\cos\tau)\dot{Y}_0$$

$$Y = \frac{tg\alpha}{\tau_D}(1-\cos\tau+\Delta\tau\sin\tau) + (1-\cos\tau+\Delta\tau\sin\tau)\dot{X}_0+Y_0+(\sin\tau+\Delta\tau\cos\tau)\dot{Y}_0 \quad (A7)$$

$$\dot{Y} = \frac{tg\alpha}{\tau_D}(\sin\tau+\Delta\tau\cos\tau) + (\sin\tau+\Delta\tau\cos\tau)\dot{X}_0+(\cos\tau-\Delta\tau\sin\tau)\dot{Y}_0$$

$$Z = Z_0 + \dot{Z}_0(\tau+\Delta\tau) + \frac{1}{2\tau_D}(\tau^2+2\tau\Delta\tau)$$

$$\dot{Z} = \dot{Z}_0 + \frac{(\tau+\Delta\tau)}{\tau_D}$$

We have retained the products $\dot{X}_0\Delta\tau$, $\dot{Y}_0\Delta\tau$, $\dot{Z}_0\Delta\tau$ since in some particular case the component of the momentum will coincide with the total momentum, like $\dot{Z}_0 = -(1+\frac{\Delta p}{p})$.

i) Motion from the plane $Z=Z_D$ to the mirror

The beam has to be traced back or forward (depending on the starting condition of the single ray) in the magnetic field only until it reaches the mirror. The grid of the mirror is defined by the equation

$$Z-Z_D = -Y tg\alpha$$

Substitution of eq (A7) gives for the transit time to first order,

$$\tau_{10} = -Y_0 tg\alpha$$

At the mirror entrance we obtain the following values for the coordinates and momentum

axis pointing along the direction of motion. (See Fig. A3)
We need to translate the coordinates by the quantity

$$X_D = -tg\alpha \; \frac{\tau_D - \sin\tau_D}{\tau_D}$$

$$Y_D = tg\alpha \; \frac{1 - \cos\tau_D}{\tau_D}$$

and then rotate the system by an angle $\tau_D/2$.

After the rotatranslation we obtain (Z and $\dot{Z}$ are un-changed)

$$X_{co} = \cos\tau_D/2 \; X_o + \sin\tau_D/2 \; Y_o + 2 \; \sin\tau_D/2 \dot{X}_o$$

$$Y_{co} = -\sin\tau_D/2 \; X_o + \cos \tau_D/2 \; Y_o - 2\sin \tau_D/2 tg\tau_D/2 \dot{X}_o + 2 tg\tau_D/2 \; \frac{\Delta p}{p}$$

$$\dot{X}_{co} = \frac{1}{\cos\tau_D/2} \; \dot{X}_o - tg\tau_D/2 \; \frac{\Delta p}{p}$$

$$\dot{Y}_{co} = 1 + \frac{\Delta p}{p}$$

$$Z_{co} = Z_2$$

$$\dot{Z}_{co} = \dot{Z}_2$$

iv) Phase space at the plane $Y_c = 0$

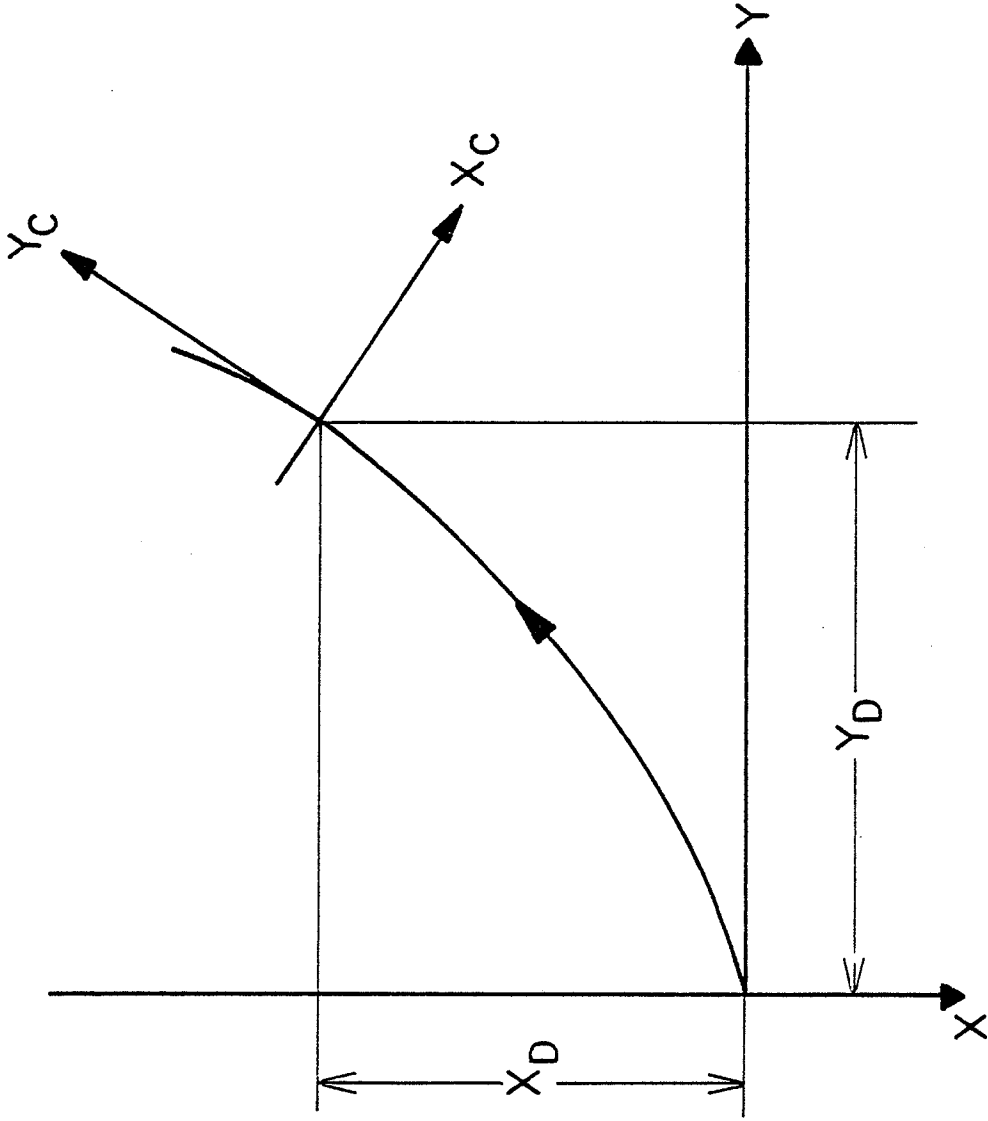The central ray at the exit of the mirror has the coordinates

FIG. A3. Coordinate system used at the mirror exit.

Forward Matrix

$$\begin{pmatrix} x_c \\ \dot{x}_c \\ z_c \\ \dot{z}_c \\ \Delta\tau \\ \dfrac{\Delta p}{p} \end{pmatrix} = \begin{pmatrix} \cos\tau_D/2 & 2\sin\tau_D/2 & \sin\tau_D/2 & 0 & 0 & 0 \\[4pt] -\sin\tau_D/2 & \dfrac{\cos\tau_D}{\cos\tau_D/2} & \cos\tau_D/2 & 0 & 0 & tg\tau_D/2 \\[10pt] 0 & 0 & -tg\alpha & 0 & 0 & -\tau_D \\[6pt] 0 & \dfrac{-tg\tau_D/2}{tg\alpha} & 0 & \dfrac{-1}{tg\alpha} & 0 & \left(\dfrac{1}{tg\alpha\cos\tau_D/2}-1\right) \\[10pt] \sin\tau_D/2 & 0 & tg\alpha-\cos\tau_D/2 & -2\sin\tau_D/2 & 1 & 0 \\[4pt] 0 & 0 & 0 & 0 & 0 & 1 \end{pmatrix} \begin{pmatrix} x_o \\ \dot{x}_o \\ y_o \\ \dot{y}_o \\ \Delta\tau_o \\ \dfrac{\Delta p}{p} \end{pmatrix}$$

Backward Matrix

$$\begin{pmatrix} x_o \\ \dot{x}_o \\ y_o \\ \dot{y}_o \\ \Delta\tau_o \\ \dfrac{\Delta p}{p} \end{pmatrix} = \begin{pmatrix} \dfrac{\cos\tau_D}{\cos\tau_D/2} & -2\sin\tau_D/2 & \dfrac{-tg\tau_D/2}{tg\alpha} & 0 & 0 & 0 \\[10pt] \sin\tau_D/2 & \cos\tau_D/2 & \dfrac{1}{tg\alpha} & 0 & 0 & \sin\tau_D/2 \\[10pt] 0 & 0 & -\dfrac{1}{tg\alpha} & 0 & 0 & -\dfrac{\tau_D}{tg\alpha} \\[10pt] -\sin\tau_D/2\,tg\tau_D/2 & -\cos\tau_D/2\,tg\tau_D/2 & \dfrac{-tg\tau_D/2}{tg\alpha} & -tg\alpha & 0 & \cos\tau_D/2-tg\alpha \\[10pt] -tg\tau_D/2 & 0 & 1-\dfrac{1}{tg\alpha\cos\tau_D/2} & -2\sin\tau_D/2\,tg\alpha & 1 & 0 \\[6pt] 0 & 0 & 0 & 0 & 0 & 1 \end{pmatrix} \begin{pmatrix} x_c \\ \dot{x}_c \\ z_c \\ \dot{z}_c \\ \Delta\tau \\ \dfrac{\Delta p}{p} \end{pmatrix}$$

$$X_{co} = 0 \qquad Y_{co} = 0 \qquad Z_{co} = 0$$

and we want to define "virtual" phase space in the cyclotron in the plane $Y_c = 0$. The transit time to the plane $Y_c = 0$ is

$$\tau_c = -Y_{co}$$

and we obtain for the motion from the plane $Z = Z_D$ to the plane $Y_c = 0$

$$Y_c = 0$$

$$\dot{Y}_c = 1 + \frac{\Delta p}{p}$$

$$X_c = \cos\tau_D/2 \; X_o + 2\sin\tau_D/2\dot{X}_o + \sin\tau_D/2 Y_o$$

$$\dot{X}_c = -\sin\tau_D/2 X_o + \frac{\cos\tau_D}{\cos\tau_D/2} \; \dot{X}_o + \cos\tau_D/2 Y_o + tg\tau_D/2 \; \frac{\Delta p}{p}$$

$$Z_c = -tg\alpha \; Y_o - \tau_D \frac{\Delta p}{p}$$

$$\dot{Z}_c = \frac{-tg\tau_D/2}{tg\alpha} \; \dot{X}_o - \frac{1}{tg\alpha} \; \dot{Y}_o + \left(\frac{1}{tg\alpha\cos\tau_D/2} -1\right) \frac{\Delta p}{p}$$

$$\tau_{co} - \tau_D = \sin\tau_D/2 \; X_o + (tg\alpha-\cos\tau_D/2)Y_o - 2\sin\tau_D/ 2 \; \dot{Y}_o$$

We can then use a matrix notation for the transformation of the phase space from the plane $Z = Z_D$ to the plane $Y_c = 0$. The forward and backward matrices will be

Appendix B

Equations of motion in an axially symmetric magnetic field

Linear equations

The equation of motion of a charged particle in a magnetic and electric field is:

$$\frac{d\vec{p}}{dt} = q\ (\vec{E} + \vec{v} \times \vec{B})\ . \tag{B1}$$

We perform a change of the independent variable from $\underline{t}$ to $\underline{z}$ through the relation

$$\frac{d}{dt} = v_z\ \frac{d}{dz}\ , \tag{B2}$$

Equation (B1) is equivalent to the following system of first order differential equations (the dot indicates derivative with respect to z)

$$\dot{x} = \frac{p_x}{p_z}$$

$$\dot{y} = \frac{p_y}{p_z}$$

$$\dot{t} = \frac{m}{p_z}$$

$$\dot{p}_x = q \left[\frac{mE_x}{p_z} + \frac{p_y}{p_z} B_z - B_y \right]$$

$$\dot{p}_y = q \left[\frac{mE_y}{p_z} + B_x - \frac{p_x}{p_z} B_z \right] \qquad (B3)$$

$$\dot{p}_z = q \left[\frac{mE_z}{p_z} + \frac{p_x}{p_z} B_y - \frac{p_y}{p_z} B_x \right]$$

For an axially symmetric field, the vector potential and field components in cylindrical coordinates are given by

$$A_r = 0 \qquad\qquad B_r = -\frac{\partial A_\theta}{\partial z}$$

$$A_z = 0 \qquad\qquad B_z = \frac{1}{r} \frac{\partial}{\partial r} (rA_\theta) \qquad (B4)$$

$$A_\theta = \frac{1}{r}\int_0^r rB_z dr \qquad B_\theta = 0$$

The θ component of the vector potential can be expressed as a series expansion in r as:

$$A_\theta = \frac{r}{2} B - \frac{r^3}{16} B'' + \ldots \qquad (B5)$$

where $B(z) = B_z(r=0,z)$ and the primes indicate derivatives with respect to z.

A first order expansion for the cartesian components of the magnetic field yields (using Eqs. B4 and B5):

$$B_z = B$$

$$B_x = -\frac{1}{2} xB' \qquad (B6)$$

$$B_y = -\frac{1}{2} y B'$$

We can now linearize the system (B3) using the expressions derived above for the fields and the first order expansion

$$p_z \approx p_o, \qquad \text{(B7)}$$

where p_o is the total momentum. Note that the sign of p_o depends on the direction of motion.

The linearized equations of motion are then:

$$\dot{x} = \frac{p_x}{p_o}$$

$$\dot{y} = \frac{p_y}{p_o}$$

$$\dot{t} = \frac{m}{p_o} \qquad \text{(B8)}$$

$$\dot{p}_x = q \left[\frac{mE_x}{p_o} + \frac{p_y}{p_o} B + \frac{1}{2} B'y \right]$$

$$\dot{p}_y = q \left[\frac{mE_y}{p_o} - \frac{1}{2} B'x - \frac{p_x}{p_o} B \right]$$

$$\dot{p}_o = q \frac{mE_z}{p_o}$$

Canonical equations of motion

Consider the motion of a charged particle in a magnetic field. A set of canonical variables in a cartesian frame is given by:

$$x, \ y, \ z$$

$$\qquad \text{(B9)}$$

$$\vec{P} = \vec{p} + q\vec{A}$$

where $\vec{P}$ is the canonical momentum, and $\vec{p}$ the linear momentum.

In the case of an axially symmetric magnetic field, the cartesian components of the vector potential are

$$A_x = - \frac{y}{r} A_\theta ,$$
$$A_y = \frac{x}{r} A_\theta ,$$
$$A_z = 0. \tag{B10}$$

Using the expansion (B5) for A_θ, we obtain the following relation between canonical and linear momentum, valid to first order:

$$P_x = p_x - \frac{1}{2} q B_y$$
$$P_y = p_y + \frac{1}{2} q B_x \tag{B11}$$
$$P_z = p_z$$

We omit in this case the electric field; the total scalar momentum is then conserved. The linearized equations of motion are (B8):

$$\dot{x} = \frac{P_x + \frac{1}{2} q By}{P_o}$$

$$\dot{y} = \frac{P_y - \frac{1}{2} q Bx}{P_o}$$

$$\tag{B12}$$

$$\dot{P}_x = \frac{1}{2} q B\dot{y}$$

$$\dot{P}_y = -\frac{1}{2} q B\dot{x}$$

53

We must point out that the motion in linear or canonical coordinates (Eqs. B8, B12) is coupled. We can however define a rotating cartesian frame (ξ, η), called Larmor frame, that makes an angle $\mu(z)$ with respect to (xy) given by

$$\mu(z) = -\frac{1}{2} \int_{z_o}^{z} \frac{qB}{p_o} dz \quad , \qquad \text{B13)}$$

where z_o is the location where the two frames coincide. We recall that B is the z-component of the magnetic field on the axis of symmetry and p_o is the total scalar momentum with sign.

The transformation between the two sets of canonical variables is

$$
\begin{vmatrix} \xi \\ P_\xi \\ \eta \\ P_\eta \end{vmatrix}
=
\begin{vmatrix}
\cos\mu & 0 & \sin\mu & 0 \\
0 & \cos\mu & 0 & \sin\mu \\
-\sin\mu & 0 & \cos\mu & 0 \\
0 & -\sin\mu & 0 & \cos\mu
\end{vmatrix}
\begin{vmatrix} x \\ P_x \\ y \\ P_y \end{vmatrix}
\qquad \text{(B14)}
$$

The equations of motion in the new variables are now

$$\dot{\xi} = \frac{P_\xi}{p_o}$$

$$\dot{P}_\xi = -\frac{1}{4} \frac{q^2 B^2}{p_o} \xi$$

$$\dot{\eta} = \frac{P_\eta}{p_o} \qquad \qquad \text{B15)}$$

$$\dot{P}_\eta = -\frac{1}{4} \frac{q^2 B^2}{p_o} \eta$$

The advantage of this transformation is that it decouples the motion in the rotating frame, simplifying the equations.

Linear vs. canonical coordinates

In the previous sections we have derived the linearized equations of motion for a charged particle in an axially symmetric magnetic field using linear and canonical coordinates.

The study of phase space areas requires the use of canonical variables. The use of the Larmor frame has the additional advantage of decoupling the motion and explicitly allowing us to study the conservation of each phase space area independently.

We have assumed that the motion of the central ray is on the axis of symmetry, i.e. the z-axis, since we have linearized the equations for the transverse coordinates.

We can, however, use a general curvilinear coordinate system to describe the motion in a static magnetic field with the arc length S of the central ray trajectory as independent variable. The general conclusion[17] is that linear and canonical transverse corrdinates coincide every time no longitudinal (in the S direction) field component exists.

We conclude therefore that the two sets of coordinates and the corresponding phase space areas coincide obviously at the injection point z = 100" (since there the magnetic field vanishes) and at the inflector exit since there the field is perpendicular to the trajectory.

We are interested in the transformation between linear and canonical coordinates in the median plane, close to the inflector entrance. Assuming a uniform field B_0 in the negative z-direction, equation (B11) becomes:

$$\frac{P_x}{p} = \frac{p_x}{p} + \frac{1}{2}\frac{y}{\rho}$$

$$\frac{P_y}{p} = \frac{p_y}{p} - \frac{1}{2}\frac{x}{\rho}$$

(B16)

where $p = qB_0\rho$ is the total linear momentum.

References

1. J. Arianer, et al., IEEE Trans. on Nucl. Sci. NS-26 (1979) 3713.

2. R. Geller, IEEE Trans. on Nucl. Sci. NS-26 (1979) 2120.

3. Y. Jongen, et al., IEEE Trans. on Nucl. Sci. NS-28 (1981) 2696.

4. V. Bechtold, et al., IEEE Trans. on Nucl. Sci. NS-26 (1979) 3680.

5. R.K. Bandhari, J. Reich, Proc. IX Intl. Conf. on Cyclotrons and Their Applications, CAEN Sept. 1981 - to be published.

6. W.K. Van Asselt, et al., Proc. IX Intl. Conf. on Cyclotrons and Their Applications, CAEN, Sept. 1981 - to be published.

7. M. Lieuvin, Proc. IX Intl. Conf. on Cyclotrons and Their Applications, CAEN, Sept. 1981 - to be published.

8. F.G. Resmini, et al., IEEE Trans. on Nucl. Sci. NS-26 (1979) 2078.

9. W.B. Powell, et al., Nucl. Instr. and Meth. 32 (1965) 325.

10. N. Hazewindus, Nucl. Instr. and Meth. 129 (1975) 325.

11. R.W. Muller, Nucl. Instr. and Meth. 54 (1967) 29.

12. J.L. Belmont, et al., IEEE Trans. on Nucl. Sci. NS13 (1966) 191.

13. E. Liukkonen, et al., IEEE Trans. on Nucl. Sci. NS-26 (1979) 2107.

14. J.S. Colonias, UCRL 18439 (1968).

15. N. Chan Tung, et al., Nucl. Instr. and Meth. 174 (1980) 151.

16. N. Hazewindus, Nucl. Instr. and Meth. 76 (1969) 273.

17. E.D. Courant and H.S. Snyder, Annals of Physics 3 (1958) 1.